JOINT TRANSPORTATION RESEARCH PROGRAM

INDIANA DEPARTMENT OF TRANSPORTATION
AND PURDUE UNIVERSITY

Receiver, Vehicle, and Roadway Systems for a Dynamic Wireless Power Transfer Roadway Testbed

Oscar Andrés Moncada, Isaac Abram, Nicholas Frooninckx, Vatan Mehar, Chiara Cervini, Ben O'Brien, Bruno Krause Moras, Steve Pekarek, John E. Haddock, Dionysios Aliprantis, Aaron Brovont, Konstantina Gkritza, and Rob Swanson

SPR-4856 • Report Number: FHWA/IN/JTRP-2026/18 • DOI: 10.5703/1288284318633

RECOMMENDED CITATION

Moncada, O. A., Abram, I., Frooninckx, N., Mehar, V., Cervini, C., O'Brien, B., Moras, B. K., Pekarek, S., Haddock, J. E., Aliprantis, D., Brovont, A., Gkritza, K., & Swanson, R. (2026). *Receiver, vehicle, and roadway systems for a dynamic wireless power transfer roadway testbed* (Joint Transportation Research Program Publication No. FHWA/IN/JTRP-2026/18). West Lafayette, IN: Purdue University. https://doi.org/10.5703/1288284318633

AUTHORS

Oscar Andrés Moncada
Lyles School of Civil and Construction Engineering
Purdue University

Isaac Abram
Elmore Family School of Electrical and Computer Engineering
Purdue University

Nicholas Frooninckx
Elmore Family School of Electrical and Computer Engineering
Purdue University

Vatan Mehar
Elmore Family School of Electrical and Computer Engineering
Purdue University

Chiara Cervini
Department of Political Science
Purdue University

Ben O'Brien
Lyles School of Civil Engineering & Department of Political Science
Purdue University

Bruno Krause Moras
Lyles School of Civil and Construction Engineering
Purdue University

Steve Pekarek
Elmore Family School of Electrical and Computer Engineering
Purdue University

John E. Haddock, PhD, PE
Lyles School of Civil and Construction Engineering
Purdue University
(765) 496-3996
jhaddock@purdue.edu
Corresponding Author

Dionysios Aliprantis
Elmore Family School of Electrical and Computer Engineering
Purdue University

Aaron Brovont
Elmore Family School of Electrical and Computer Engineering
Purdue University

Konstantina Gkritza
Lyles School of Civil and Construction Engineering
Purdue University

Rob Swanson
Elmore Family School of Electrical and Computer Engineering
Purdue University

JOINT TRANSPORTATION RESEARCH PROGRAM

The Joint Transportation Research Program serves as a vehicle for INDOT collaboration with higher education institutions and industry in Indiana to facilitate innovation that results in continuous improvement in the planning, design, construction, operation, management and economic efficiency of the Indiana transportation infrastructure. Learn more at engineering.purdue.edu/JTRP.

Published reports of the Joint Transportation Research Program are available at docs.lib.purdue.edu/jtrp/.

NOTICE

TECHNICAL REPORT DOCUMENTATION PAGE

1. Report No.	2. Government Accession No.	3. Recipient's Catalog No.
FHWA/IN/JTRP-2026/18		

4. Title and Subtitle Receiver, vehicle, and roadway systems for a dynamic wireless power transfer roadway testbed	**5. Report Date** May 21, 2026 **6. Performing Organization Code**
7. Author(s) Oscar Andrés Moncada (https://orcid.org/0009-0003-3826-1011) Isaac Abram (https://orcid.org/0009-0002-6239-0377) Nicholas Frooninckx (https://orcid.org/0009-0002-3363-9022) Vatan Mehar (https://orcid.org/0000-0001-5730-1697) Chiara Cervini (https://orcid.org/0009-0005-1803-2603) Ben O'Brien (https://orcid.org/0009-0009-0855-5290) Bruno Cesar Krause Moras (https://orcid.org/0009-0003-1243-1238) Steve Pekarek (https://orcid.org/0000-0001-6754-852X) John E. Haddock, PhD, PE (https://orcid.org/0000-0002-8030-317X) Dionysios Aliprantis (https://orcid.org/0000-0003-4255-4944) Aaron Brovont (https://orcid.org/0000-0003-3171-8042) Konstantina Gkritza (https://orcid.org/0000-0002-6598-4771) Rob Swanson (https://orcid.org/0009-0004-2374-8190)	**8. Performing Organization Report No.** FHWA/IN/JTRP-2026/18
9. Performing Organization Name and Address Joint Transportation Research Program Hall for Discovery and Learning Research (DLR), Suite 204 207 S. Martin Jischke Drive West Lafayette, IN 47907	**10. Work Unit No.** **11. Contract or Grant No.** SPR-4856
12. Sponsoring Agency Name and Address Indiana Department of Transportation (SPR) State Office Building 100 North Senate Avenue Indianapolis, IN 46204	**13. Type of Report and Period Covered** Final Report **14. Sponsoring Agency Code**

15. Supplementary Notes

Conducted in cooperation with the U.S. Department of Transportation, Federal Highway Administration.

16. Abstract

A dynamic wireless power transfer (DWPT) system using a novel three-phase transmitter/receiver design was embedded 2.4 in. beneath the surface of an existing rigid pavement on US 52/US 231 in West Lafayette, Indiana, with 85 coils installed and paired with a retrofitted Class 8 Cummins electrified truck. The system successfully delivered 50–190 kW at speeds up to 65 mph with efficiencies approaching 85%, and all coils met electromagnetic balance targets; similar results were validated on a 3-coil testbed at Utah State University, with magnetic flux densities well below human exposure limits. Testing also demonstrated strong misalignment tolerance and reliable high-power delivery without active vehicle-roadway alignment technologies. In addition, the project conducted extensive public outreach in collaboration with INDOT to inform and engage the community.

17. Key Words	18. Distribution Statement
dynamic wireless power transfer, electric trucks, concrete, rigid pavement, field testing, public outreach	No restrictions. This document is available through the National Technical Information Service, Springfield, VA 22161.

19. Security Classif. (of this report)	20. Security Classif. (of this page)	21. No. of Pages	22. Price
Unclassified	Unclassified	36	

Form DOT F 1700.7 (8-72) Reproduction of completed page authorized

EXECUTIVE SUMMARY

Introduction

In this research, focus has been placed on the development of a dynamic wireless power transfer (DWPT) system in which a roadway provides power to an electrified freight vehicle (e.g. Class-8 truck) while it moves at highway speeds. The promise of DWPT is that it enables a significant reduction in the battery required and the need for drivers to stop and refuel/recharge, leading to a significant reduction in the total cost of ownership, higher asset utilization, and a lower cost of goods and services. Key technical challenges of creating a DWPT system capable of serving freight vehicles are the high level of power (~180 kW) required, the fact that the transmitter coils must be buried well below the roadway surface to enable roadway maintenance, and that an appreciable ground clearance must be maintained between the roadway and the DWPT receiver to ensure vehicle integrity.

Under this study, a DWPT system was designed that leverages a novel three-phase transmitter/receiver system to meet these challenges. The system was designed to be installed within an existing concrete pavement with transmitter coils placed 2.4 in. below the roadway surface in milled channels. A roadway-to-receiver ground clearance of 8 in. was specified. The design was then instantiated through the development of an 85-coil DWPT testbed on US 52/231 in West Lafayette, Indiana. A Class-8 Cummins electrified vehicle was retrofitted with a DWPT receiver system to serve as a test vehicle. Here, a key aspect of the design was that the receiver system could only occupy space under the tractor vehicle, not the trailer. In tandem with the 85-coil testbed, the team also instantiated a three-coil version of the testbed at Utah State University (USU) to support the development of standards for DWPT systems.

Public perception remains a critical factor in the successful deployment and societal integration of such technologies. Without proactive engagement and community support, innovations like DWPT may encounter resistance that could impede their implementation. In collaboration with the Indiana Department of Transportation (INDOT) and alongside roadway construction, the team developed a comprehensive suite of outreach materials—including presentations, media content, a dedicated project webpage, and survey instruments—to facilitate public engagement in the vicinity of the Indiana DWPT testbed and across other regions of the state.

Findings

This report documents the tasks the team performed to support the testbed instantiation and validation, and the use of the testbed to engage the community and understand their understandings/perceptions of the technology. Highlights include that all 85 coils met the target electromagnetic performance specifications used to enforce balance between the voltages/currents of the three-phase coils. This was a significant result as a key question surrounding the three-phase coil topology was whether the relatively precise separation distance between phase coils used to establish balance could be maintained through a multistage construction process. Most importantly, the roadway was shown to efficiently provide the power commanded by the Cummins system control module, from 50 kW to 190 kW at vehicle speeds of up to 65 mph. System efficiency, taken from the roadway direct current (DC)-bus to the vehicle DC-bus, was measured to approach 85% at peak power. Nearly identical system performance was observed in the three-coil testbed at USU, where measurements performed by an independent testing group validated that the magnetic flux density values were well below the 15 μT level set for human exposure limits.

A public information session and an open house were held, drawing a strong turnout from local residents. Survey findings suggest that the public perceives DWPT as beneficial for improving local air quality and mitigating range anxiety associated with electrified vehicles. Nonetheless, open-ended responses highlighted concerns regarding the allocation of public funds to technologies perceived as serving a limited demographic. Conversely, several participants expressed strong support for the pilot, citing deficiencies in the existing charging infrastructure as a barrier to broader electric vehicle (EV) adoption. Notably, some respondents viewed DWPT as a catalyst for accelerating the transition to alternative energy sources, including nuclear power.

Implementation/Lessons Learned

The performance of a DWPT system was evaluated through design and construction of the 85-coil testbed on US 52/231. Overall, the system behaved as designed and the models derived as the basis for creating system specifications have been validated. Several lessons were learned through the entire testbed development process. These include:

- Installing DWPT as a retrofit in a concrete pavement system is cost prohibitive. The multiple stages involved to accurately mill channels, perform vertical and horizontal boring for conduit placement, and install vaults in the foreslope require significant time, specialized equipment, and extensive manpower. INDOT envisions future DWPT installations could leverage precast solutions to create electrified roadways, which is compatible with the three-phase system that has been developed. Our team has also designed a slip-form strategy that we believe would be a relatively low-cost means to install the systems in new pavement installations.
- The team specified each turn of each three-phase transmitter coil be terminated at its inverter to reduce voltage levels within the compensation circuit. This required termination of 12 Litz-conductor leads per transmitter coil, which added significant time and cost to the project. The time/cost far exceeded the savings gained in reducing voltage levels within the compensation circuits. In future installations, a neutral point would be created within each transmitter coil and only three leads would be brought back for inverter termination. The three-lead termination will result in a 50% reduction in Litz terminations, a 25% reduction in Litz wire required, and a 75% reduction in the number of

inverter enclosure penetrations, which will greatly reduce the cost to meet IP68 water ingress requirements.

- A significant cost of high-power DWPT systems is the inverters used to create the high-frequency alternating current (AC) signals provided to the transmitter coils. To minimize risk, we specified an inverter per transmitter coil for the DWPT testbed. Research performed through this project has led to new system design approaches where multiple coils can be fed from a single inverter enclosure, which is projected to greatly reduce DWPT system cost.
- A diesel mobile generator was initially utilized to power the primary supply to the testbed. In the early stages of the acceptance testing process, when few inverters were on the DC-bus, there was relatively little capacitive energy storage to help maintain the DC-bus voltage during transients. In testing the trip response of the first inverters installed, the low energy storage in combination with the slow response time of the generator led to system voltages that exceeded ratings and damaged an inverter. To remedy this, a power source with a faster transient response time can be used to minimize the voltage excursion. To this end, the original mechanical diesel generator was replaced by an active battery energy storage system in the testbed. This battery system provided much faster response times to load changes of the system, effectively eliminating the voltage transients observed when the generator was used.
- The testbed/test vehicle did not use any technologies to promote alignment between the vehicle receiver and the roadway transmitters. Despite this, in all testing performed to date, the roadway was able to provide the power requested by the test vehicle, which we believe demonstrates the robust misalignment performance of the three-phase transmitter/receiver system.
- The study proposes key public education/outreach framing strategies, including presenting DWPT as a shared public investment with transparent financial benefits, clearly communicating construction impacts and mitigation efforts, and positioning the technology as a solution to major EV adoption barriers such as charging access, time, and cost. It also stresses the importance of explaining technical and safety aspects in relatable terms to improve public understanding. While supported by prior research, the recommendations are intended as a high-level starting point rather than a comprehensive outreach blueprint.

CONTENTS

LIST OF TABLES

LIST OF FIGURES

1. INTRODUCTION

This report documents the primary tasks associated with design, construction, and initial testing of a dynamic wireless power transfer (DWPT) testbed (DWPTT) in the northbound rightmost lane of US Route (US) 52/231 in West Lafayette, Indiana, USA. Figure 1.1 provides a conceptual illustration of the testbed, including the main components that are part of the system (Aliprantis et al., 2025). The testbed extends approximately 1,300 ft along an existing rigid-pavement (concrete) roadway, specifically the northbound, rightmost lane. Embedded roughly 2.4 in. below the roadway surface are 85 three-phase transmitter coils. These coils are powered by 85 inverters, each housed in one of 43 subsurface concrete vaults located in the adjacent roadway foreslope, with each vault containing two inverters (one per coil). To mitigate the weak coupling between transmitter and receiver coils—separated by approximately 10.5 in. and lacking any intervening magnetic material—compensation circuits are integrated within the inverters.

An electrical diagram of the testbed is shown in Figure 1.2. Therein it can be seen that the inverters are rated for 230 kW and are powered by a 750-V DC bus that runs the length of the roadway. This DC bus is supplied by a battery energy storage system (BESS), whose direct current (DC)–alternating current (AC) conversion stage generates a three-phase, 480-V, 60-Hz AC bus. The AC output is then stepped up and rectified via a three-phase to six-phase (delta-wye) transformer feeding a 12-pulse diode rectifier, which produces the 750 V DC required for the inverters. Ethernet communication is used for monitoring and controlling the inverters. In addition, fiber-optic links between inverters transmit activation signals based on the sensed power draw of the preceding inverter. These links also ensure synchronization of the voltage waveforms during vehicle transitions between adjacent transmitters, enabling seamless power delivery in motion.

In addition to the electrical components in the roadway, Figure 1.2 shows a receiver-side system that is placed on a vehicle to accept power from the transmitter coils and provide the power to the vehicle electrical system that includes the battery, propulsion drive, and auxiliary equipment. The receiver-side system was also developed under this program and integrated into a Class-8 electric vehicle (EV) provided by Cummins to serve as a test vehicle for the testbed.

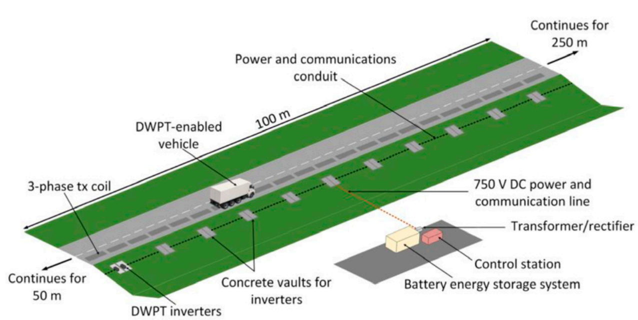

Figure 1.1 Conceptual Overview of the Indiana Dynamic Wireless Power Transfer Testbed (DWPTT).

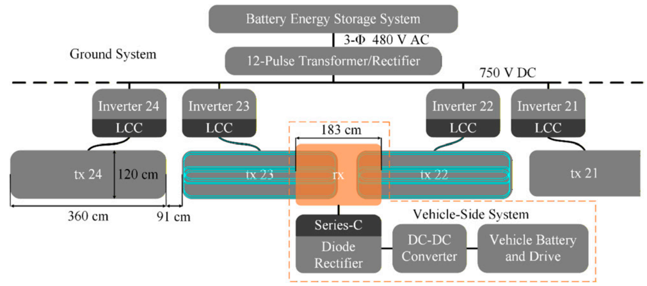

Figure 1.2 Electrical System Diagram. Four Consecutive Transmitters (tx) Are Shown. The Receiver (rx), Which is Mounted Under the Truck That Moves From Right to Left, Has a Similar Three-Phase Topology as the tx, but its Dimensions Are Different.

All the components shown in Figure 1.1 and Figure 1.2 have been successfully installed in the testbed. Data from roadway testing have demonstrated that all 85 coils met the target electromagnetic performance specifications used to enforce balance between the voltages/currents of the three-phase coils. Most importantly, the roadway has been shown to efficiently provide the power commanded by the Cummins system control module, from 50 kW to 190 kW at vehicle speeds of up to 65 mph. System efficiency, taken from the roadway DC-bus, to the DC-bus of the vehicle, was measured to approach 85% at peak power.

To systematically assess public sentiment, a survey (Purdue IRB-2023-786) was administered in the Greater Lafayette area during the testbed construction phase. The instrument gauged respondents' familiarity with EVs and various charging modalities, including DWPT. Screening and verification questions were incorporated to ensure data integrity, resulting in 275 valid responses. Survey findings suggest that the public perceives DWPT as beneficial for improving local air quality and mitigating range anxiety associated with EVs. Nonetheless, open-ended responses highlighted concerns regarding the allocation of public funds to technologies perceived as serving a limited demographic. Conversely, several participants expressed strong support for the pilot, citing deficiencies in the existing charging infrastructure as a barrier to broader EV adoption. Even among proponents of DWPT, apprehensions were noted regarding noise pollution, traffic disruptions during construction, and the broader implications of scaling the technology. Notably, some respondents viewed DWPT as a catalyst for accelerating the transition to alternative energy sources, including nuclear power.

2. PAVEMENT SECTION & CONSTRUCTION

2.1 Pavement Section Design

The DWPT testbed was constructed within an existing jointed plain concrete pavement (JPCP) roadway located along the northbound right lane of US Route (US) 52/231 in West Lafayette, Indiana. The roadway segment selected for the testbed consists of a series of concrete slabs that were retrofitted to incorporate the embedded DWPT transmitter systems while preserving the structural integrity of the pavement structure. The testbed extends approximately 1,300 ft along the roadway and

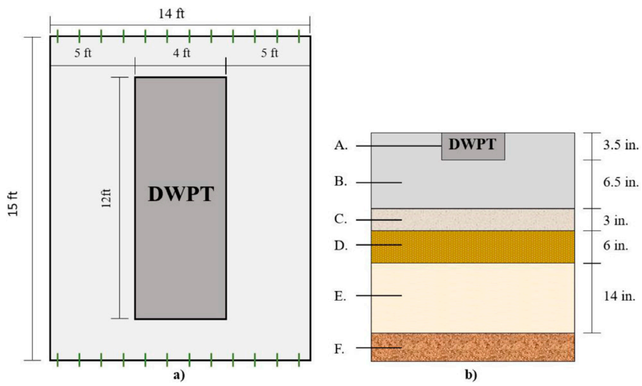

Figure 2.1 (a) Plan View of the DWPT Testbed Pavement Section and (b) Cross-Section of the Pavement Structure.

TABLE 2.1
Layer Configuration of the DWPT Testbed Pavement Section.

ID	Thickness	Pavement Layer
A	3.5 in.	Polyester concrete (DWPT channel)
B	10 in.	PCC
C	3 in.	#8 Open grade AGG base
D	6 in.	#53 Dense AGG subbase
E	14 in.	Soil treatment
F	--	Soil subgrade

includes a total of 85 transmitter installations distributed longitudinally along the traffic lane. Each concrete slab containing a DWPT transmitter measures 14 ft in width and 15 ft in length, as shown in Figure 2.1a. The existing pavement structure at the testbed site consists of a 10-in. thick Portland Cement Concrete (PCC) slab constructed over a 3-in. #8 open-graded aggregate (AGG) base course, a 6-in. #53 dense AGG subbase layer, and a 14-in. soil treatment layer above the natural soil subgrade, as illustrated in Figure 2.1b and detailed in Table 2.1. The DWPT transmitter channel measures 4 ft in width, 12 ft in length, and is embedded within the PCC slab at a depth of approximately 3.5 in. below the pavement surface. Within each PCC slab, the DWPT transmitter channel is centered laterally within the traffic lane, leaving approximately 5 ft of concrete on each side of the DWPT channel in the transverse direction and approximately 1.5 ft in the longitudinal direction. The DWPT channel is filled with polyester concrete, which was selected for its adhesive properties and compatibility with the surrounding PCC slab. The existing JPCP is a jointed plain concrete pavement with transverse contraction joints spaced at regular intervals, dividing the roadway into individual slab panels. These joints are equipped with steel dowel bars to facilitate load transfer across the joints. Each dowel bar is approximately 18 in. in length and 1.5 in. in diameter, centered on the joint at middepth of the slab.

2.2 Roadway Construction

Construction of the testbed involved retrofitting the PCC panels within the existing JPCP roadway to accommodate the embedded DWPT channels and associated electrical

Figure 2.2 (a) DWPT Channel Milling Within PCC Panels and (b) Conventional Milling Machine Used for Channel Construction.

infrastructure. Installation was performed in a staged sequence beginning with pavement modification, followed by electrical system installation, and concluding with pavement surface restoration. Construction began with milling of the DWPT channel within the PCC slabs, as shown in Figure 2.2a. The milling created a longitudinal channel approximately 4 ft in width, 12 ft in length, and 4 in. in depth to accommodate the DWPT transmitter system. Milling operations were carried out using a conventional milling machine, as shown in Figure 2.2b, while avoiding interference with transverse contraction joints and the dowel bars located at middepth of the PCC slabs.

Stub-out coring was performed after completion of DWPT channel milling to establish conduit transitions between the DWPT channel and the roadside vault system. Two coring operations were required to accommodate conduit installation and electrical lead routing. First, a 12-in. diameter core cut was made using a compact track loader equipped with a hydraulically driven core-drilling attachment mounted on a stabilization frame, as shown in Figure 2.3a. This operation created the initial conduit pathway through the pavement layers. A 4-ft-deep larger access opening was then formed within the DWPT channel using a 42-in. diameter circular core. A circular core was used instead of a square opening to reduce stress concentrations associated with corner geometry and to minimize the potential for reflective cracking. The large-diameter coring was performed using a manhole cutting head mounted to a skid-steer platform, similar to equipment commonly used for manhole installations, as shown in Figure 2.3b. The 42-in. opening provided sufficient workspace for routing DWPT transmitter leads from the channel into the conduit that extended vertically through the pavement layers, before transitioning horizontally toward the vault structures located along the roadway foreslope, as shown in Figure 2.3c.

Trenching was then performed along the roadway shoulder and foreslope to install conduit between vault locations. Trenching was completed using a ride-on chain trencher to create narrow, continuous trenches, as shown in Figure 2.4a. The conduit installed within the trench network provided routing for power supply cables, communication lines, and DWPT control wiring between vault locations and the DWPT system. Horizontal boring was performed to connect the DWPT channel stub-outs with the trench conduit network and vault structures. A horizontal directional drilling (HDD) rig positioned along the roadway foreslope was used to install conduit beneath the PCC

(a) (b) (c)

Figure 2.3 Stub-Out Coring Operations: (a) 12-in. Diameter Vertical Core Drilling Using a Hydraulically Driven Coring Attachment, (b) 42-in. Diameter Circular Access Opening Using a Manhole Cutting Head, and (c) Completed Access Opening Within the DWPT Channel.

(a) (b)

Figure 2.4 Trenching Operations for Conduit Installation: (a) Ride-On Chain Trencher Used for Trench Excavation and (b) Completed Trench Prepared for Conduit Placement.

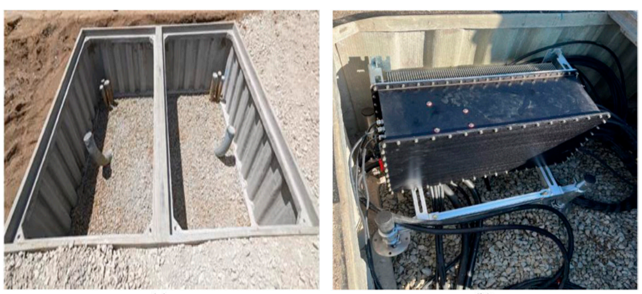

(a) (b)

Figure 2.5 (a) Vault for Housing DWPT Testbed Components in the Roadway Foreslope, and (b) Installed Inverter Within the Vault.

pavement, as shown in Figure 2.4b. The HDD operation created a bore from the foreslope toward the vertical stub-out openings to establish a horizontal conduit pathway.

Following conduit installation, concrete vaults were installed in the foreslope, cables were routed, and inverters were mounted on stands to keep them elevated above the stone base within the vaults. Figure 2.5a shows a vault after installation, where the conduits for two inverters are visible. An inverter installed within a vault is shown in Figure 2.5b.

The DWPT transmitter assemblies were installed within the milled DWPT channels, as shown in Figure 2.6a. Each transmitter assembly consists of multiple conductors arranged into

(a) (b)

Figure 2.6 DWPT Transmitter Installation and Pavement Restoration: (a) DWPT Transmitter Assemblies Placed Within the Milled Channel Prior to Concrete Placement and (b) DWPT Channel After Polyester Concrete Placement and Surface Restoration.

rectangular coil loops extending along the 12-ft channel length. Conductor spacing and alignment were maintained using a fiberglass and plastic rail support system that remained embedded within the DWPT channel. Coil testing was performed after placement to verify electrical continuity and confirm proper conductor positioning. After completion of transmitter installation and testing, the DWPT channel was filled with polyester concrete to secure the transmitter assembly and restore the PCC surface. The polyester concrete was finished to match the elevation and texture of the adjacent pavement to provide a uniform riding surface across the installation area, as shown in Figure 2.6b.

3. ROADWAY TESTING: STRUCTURAL (TASK 1)

Structural testing activities were conducted to evaluate the mechanical behavior of the roadway testbed following installation of the embedded DWPT infrastructure. These testing activities helped establish baseline structural response characteristics, enabling quantitative assessment of performance degradation rates, pavement condition evolution, and maintenance intervention effectiveness over the testbed service life. Roadway testing consisted of falling weight deflectometer (FWD) and three-dimensional (3D) ground-penetrating radar (GPR) surveys

(a) (b)

Figure 3.1 (a) Falling Weight Deflectometer Vehicle and (b) 3D Ground-Penetrating Radar Vehicle.

to characterize pavement load-response behavior, verify the internal structural condition of the roadway system after construction, and support development of a long-term dataset for pavement management applications.

The FWD, shown in Figure 3.1a, is a nondestructive testing method used to simulate a wheel load traveling over the pavement while measuring the resulting vertical surface deflection response (Park et al., 2024). The equipment applies three impulse load levels (7000 lb, 9000 lb, and 11000 lb) through separate testing sequences. During each load application, surface deflections are measured at nine sensor locations using geophones positioned at increasing radial distances from the FWD loading plate, which represents the load application point. The measured deflection data is used to assess pavement stiffness, structural capacity, and potential signs of structural deterioration. GPR scanning was used as a complementary technique to evaluate subsurface pavement conditions. This device transmits electromagnetic signals into the pavement structure and records reflected responses from material interfaces and embedded components. In this study, a 3D GPR system equipped with a vehicle-mounted antenna array (Figure 3.1b) collected spatially dense data as the vehicle traversed the test section.

Structural testing was conducted during two separate evaluation phases following completion of construction activities. The first phase of testing was performed immediately after construction of the DWPT roadway testbed and reopening of the roadway to traffic. During this phase, FWD testing was performed on 12 randomly selected slabs from the 85 total set of slabs containing DWPT coils. For each selected slab, FWD measurements were collected along two longitudinal testing paths, including one path located over the center of the DWPT unit (Path A) and one path located along the edge of the DWPT unit (Path B). Along each testing path, FWD measurements were collected at three longitudinal points: near the lower slab edge (Point 1), at the slab midlength (Point 2), and at an upper point located between the slab midlength and the upper slab edge (Point 3), as shown in Figure 3.2. Deflection measurements were recorded at each test location to document pavement load-response behavior following installation of the embedded DWPT infrastructure.

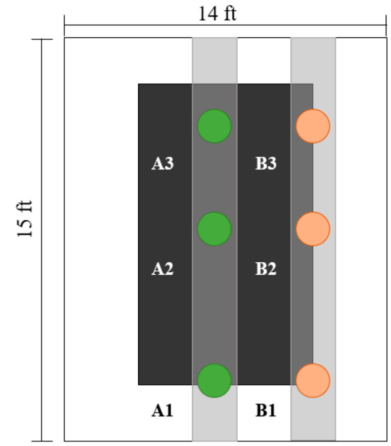

Figure 3.2 FWD Testing Layout Showing Load Locations Along Two Longitudinal Paths: Slab Center (Path A) and DWPT Edge (Path B).

During the second evaluation phase, conducted approximately eight months after construction, FWD testing was repeated at the same slabs and testing locations evaluated during the initial phase to allow direct comparison of pavement structural response over time. In addition to FWD testing, a 3D GPR survey was conducted across the DWPT testbed during the second monitoring period. The GPR survey was performed once during the second evaluation phase and covered the roadway test section using a vehicle-mounted antenna array that collected continuous subsurface data as the survey vehicle traversed the testbed. The GPR data collection was performed to document pavement layer continuity and to screen for subsurface anomalies within the DWPT slabs following early operational service of the roadway.

3.1 Observed Surface Distress and Maintenance Intervention

During the first monitoring visit, a semicircular shrinkage crack was observed across several slabs of the DWPT testbed, as observed in Figure 3.3a. The crack trace matched the perimeter of the 42-in. diameter circular coring performed to create the conduit stub-out access opening for DWPT leads, as shown in Figure 3.3b. The stub-out operation required an approximately 4-ft-deep bore, and the resulting void was backfilled with aggregate to approximately 10 in. below the surface (i.e., directly beneath the concrete layer). Because achieving uniform compaction and densification of the backfill within a confined bore was challenging, the backfilled zone provided lower support stiffness than the surrounding undisturbed foundation. This created a localized support discontinuity at the slab–foundation interface that increased slab bending susceptibility under early-age shrinkage/curling movements and initial traffic loading. Under these conditions, tensile stresses concentrated around the perimeter of the circular backfilled area, resulting in a semicircular shrinkage crack that followed the coring geometry. To address the observed distress, a low-viscosity epoxy treatment was introduced to penetrate and seal the crack network. This treatment was intended to re-establish continuity across the

(a) (b)

Figure 3.3 (a) Semicircular Shrinkage Crack Observed During the First Monitoring Visit on the DWPT Testbed; (b) 42-in. Diameter Conduit Stub-Out Access Opening (Cored) Associated With the Crack Geometry.

cracked region, limit water and incompressible intrusion, and reduce the potential for further crack opening and localized deterioration under environmental exposure and traffic.

3.2 Falling Weight Deflectometer

Figure 3.4 presents the average FWD deflection-basin curves for the DWPT center path (Path A) and edge path (Path B) for two monitoring campaigns (FWD1 and FWD2). The FWD1 dataset (solid lines) corresponds to the first monitoring visit when the semicircular crack was first detected, whereas the FWD2 dataset (dashed lines) was collected after the crack was sealed using an epoxy treatment. Deflection basin curves summarize the pavement surface response to an FWD impulse load by reporting the vertical deflection measured directly beneath the load plate and at increasing sensor offsets from the load center. In Figure 3.4, the horizontal axis is the offset distance (in.) from the load centerline, where 0 in. corresponds to the load plate location (D0) and positive offsets represent sensors located progressively farther from the load application point.

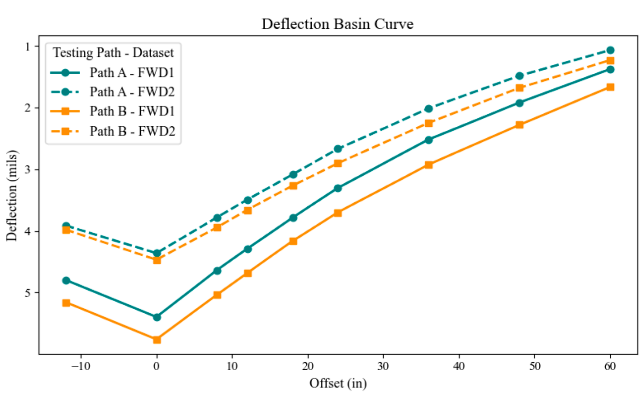

Figure 3.4 Average FWD Deflection Basin Curves for the DWPT Center Path (Path A) and Edge Path (Path B); Solid Lines Represent FWD1 and Dashed Lines Represent FWD2.

The vertical axis represents the measured surface deflection (mils), where larger values indicate greater vertical displacement of the pavement under the applied load; the maximum surface response typically occurs at D0. Across both datasets, the FWD1 basin exhibited larger deflections than FWD2 over the full offset range, with the largest difference observed at D0. For the DWPT center path (Path A), deflections at D0 decreased from approximately 5.40 mils during FWD1 to approximately 4.36 mils during FWD2, representing approximately a 19.2% difference. On the other hand, for the Path B, the deflections at D0 decreased from approximately 5.76 mils during FWD1 to approximately 4.47 mils during FWD2, representing approximately a 22.4% difference. The higher deflections measured during FWD1 are associated with the presence of the semicircular shrinkage crack within the loaded region, which reduced slab–support interaction and load-transfer efficiency, resulting in increased vertical surface response, particularly at D0. The lower deflections measured during FWD2 are attributed to the epoxy treatment, which limited crack movement and improved structural continuity across the cracked region.

Figure 3.5 compares the point-to-point deflection basin curves within each tested path (A: DWPT center; B: DWPT edge) for the two monitoring campaigns. For each path, Point 1 is the lower slab location near the slab edge, Point 2 is the slab midlength location, and Point 3 is the upper location positioned between the slab midlength and the upper slab edge. Across both testing paths, the deflection magnitudes recorded during the FWD1 campaign (solid lines) are consistently higher than those measured during the FWD2 campaign (dashed lines). For FWD1, Point 2 exhibits the largest deflection level among the three points in both paths, consistent with maximum slab bending occurring at the midlength location. Along Path B, Point 2 reaches approximately 6.5 mils, compared to approximately 6.0 mils along Path A—a modest difference of 0.5 mils. In contrast, Points 1 and 3 exhibit comparable deflection magnitudes between Paths A and B, with only minor variation between the two paths. The elevated deflection at Point 2 for both paths during FWD1 reflects the combined influence of midslab bending and crack-induced support loss, with the slight edge-center difference potentially reflecting spatial variations in crack severity or local support conditions across the testbed. Following epoxy treatment, the FWD2 measurements show convergence of deflection responses across all three-point locations, with Points 1, 2, and 3 exhibiting similar magnitudes within each path, indicating more uniform structural behavior and successful crack stabilization. Deflection values below 8 mils are generally considered indicative of adequate structural performance; the measured values across both monitoring campaigns remained within this range, confirming that the pavement is performing within acceptable structural limits.

While the semicircular shrinkage crack originated from the conduit stub-out coring region rather than at the DWPT channel edge itself, the FWD deflection data reveal a modest edge-center difference, with Path B (DWPT edge) showing slightly higher deflections than Path A (DWPT center) at

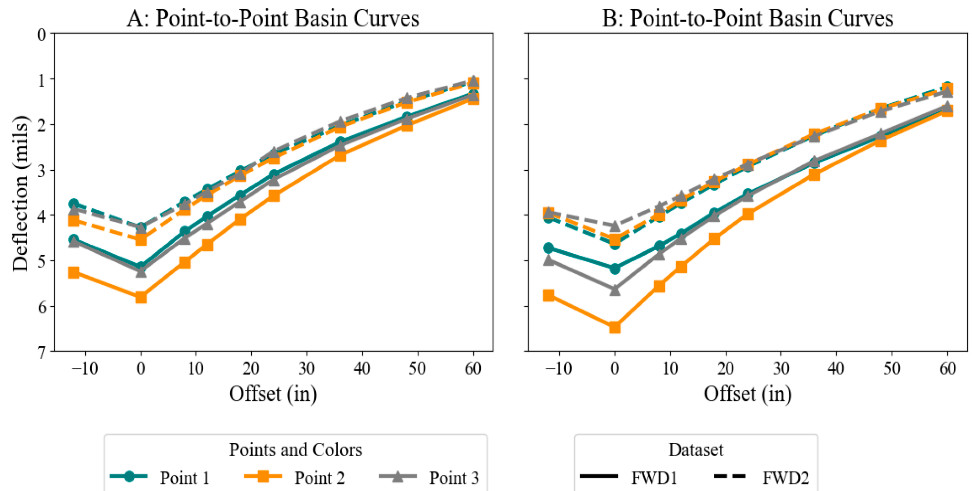

Figure 3.5 Point-to-Point FWD Deflection-Basin Curves Measured at Three Slab Locations (Points 1–3) Along (a) the DWPT Center Path (Path A) and (b) the DWPT Edge Path (Path B) for Two Monitoring Campaigns (FWD1: Solid Lines; FWD2: Dashed Lines).

Point 2 (6.5 mils versus 6.0 mils during FWD1). This 0.5 mil difference, representing approximately 8% variation, is small relative to the overall deflection magnitude and likely reflects spatial variations in how the crack and associated support loss affect local slab-foundation interaction across the testbed. From a long-term performance perspective, the channel edge merits continued monitoring attention given that material interfaces represent potential vulnerability zones in composite pavement systems. Previous full-scale rigid DWPT research has identified the channel edge as a critical interface where material property transitions can localize strain and stress concentrations under traffic loading, potentially increasing susceptibility to crack initiation and propagation (Moncada et al., 2024). Complementary finite element studies demonstrate that interface debonding conditions can significantly amplify deflection and strain responses near the DWPT-PCC boundary (Moncada et al., 2025). While the present testbed has not exhibited interface-driven distress, these established mechanisms highlight the value of monitoring the DWPT edge response to detect potential interface degradation before it manifests as structural deterioration. The epoxy treatment applied after FWD1 appears to have stabilized the crack, as evidenced by reduced deflections during FWD2 across all test locations.

3.3 3D Ground-Penetrating Radar

Figure 3.6 presents representative 3D GPR profiles collected across the DWPT roadway testbed during the second monitoring campaign (concurrent with FWD2 testing). The upper panel displays the longitudinal radargram (Figure 3.6a), showing subsurface reflections along the roadway length as a function of depth. The lower panel (Figure 3.6b), shows the transverse (width) slice extracted at a selected depth, illustrating lateral reflector patterns across the slab width, while the right-side (Figure 3.6c) trace plots display signal amplitude variations with depth at the selected crossline location. Within the longitudinal radargram, continuous horizontal reflectors near the surface correspond to the PCC slab and underlying layer interfaces. The DWPT channel region is identifiable by a distinct reflector pattern at consistent depth relative to the pavement surface, representing the material interface between the polyester concrete DWPT unit and the surrounding PCC slab. These DWPT-related reflector signatures remain visible and continuous up to approximately 1,110 ft along the x-axis, beyond which the reflector pattern transitions to that of conventional JPCP, consistent with the termination of the DWPT testbed. Throughout the scanned region, the subsurface reflectors associated with the PCC slab, DWPT channel interface, and supporting layers exhibit continuous horizontal banding without disrupted reflector geometry, hyperbolic anomaly signatures, or localized signal scattering patterns.

The GPR survey was conducted following the application of epoxy treatment to the semicircular surface crack documented during the first monitoring visit. While the footprint of the surface crack remained visible at the pavement surface, the GPR data indicated that the crack has not propagated deeply into the pavement structure. The absence of disrupted reflectors, signal attenuation zones, or hyperbolic anomaly signatures beneath the cracked region suggests that the crack depth remained confined to the upper portion of the PCC slab and did not extend through the full slab thickness or compromise the underlying layer interfaces. This finding is consistent with the crack mechanism—tensile stresses induced by localized support discontinuity at the conduit stub-out backfill zone—which would primarily affect the upper slab region under early-age shrinkage and initial traffic loading. The GPR results support the effectiveness of the epoxy treatment in limiting crack propagation, consistent with the reduced deflection response observed during FWD2 testing. Similar to the FWD baseline dataset, the GPR survey establishes a reference subsurface condition profile that enables future monitoring campaigns to detect changes

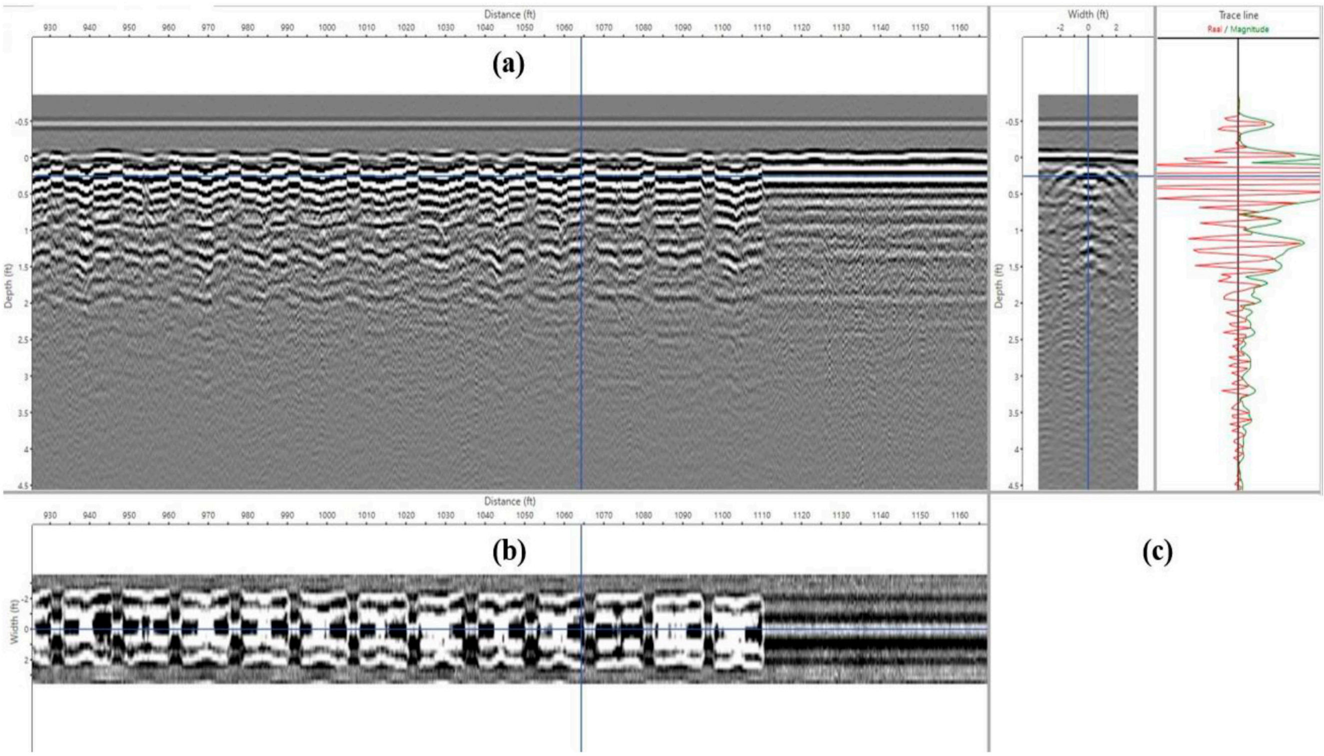

Figure 3.6 Representative 3D GPR Profile of the DWPT Roadway Testbed: (a) Longitudinal Radargram, (b) Transverse Width Slice, and (c) Trace Amplitude Response. DWPT Reflector Signatures Are Visible to Approximately Distance ≈ 1110 ft, Transitioning to Conventional JPCP Beyond This Location.

in reflector continuity, signal attenuation, or anomaly development that may indicate evolving crack penetration, interface degradation, or other internal distress within the DWPT testbed over time.

4. COMMERCIAL INSTALLATION SUPPORT (TASK 2)

Task 2 details the integration of the transmitter (tx) coils within the roadway infrastructure. From an electromagnetic standpoint, the spatial orientation of the coil conductors and end-turns needs to be precisely maintained during the installation and pouring of concrete. To achieve this, a specialized rail-rung structural system and pattern plate (Figure 4.1a and Figure 4.1b) were developed to place the windings and prevent conductor migration during installation. The rungs feature tapped holes that are spaced to the designed conductor spacing values, while the spanning rails hold the assembly under tension. The leads of each phase are wound to converge at the center of the assembly where they enter a conduit directed toward the roadside electronics enclosure. The pattern plate ensures the precise placement of these lead sections, facilitating a tight twisted bundle configuration that minimizes parasitic lead inductance and maintains uniform impedance across the installation.

An important metric for evaluating these tx coils is the Transmitter Sequence Coupling Factor (TSCF). The TSCF is a quantitative measure of electromagnetic asymmetry within the tx coils calculated using the Test Apparatus's (TA) impedance measurements. As this factor increases, it correlates with an imbalance in the coil voltages/currents and potentially the power loss in the roadway power electronics. Through the design process, a target TSCF of 5% was determined to yield acceptable performance. To validate the coils were installed correctly and that the electrical integrity was maintained, a custom TA seen in Figure 4.2 was developed to perform rapid characterization of coil impedances (Abram et al., 2025). The TA allowed for the efficient calculation of the TSCF, providing immediate feedback on whether a coil met the 5% TSCF threshold.

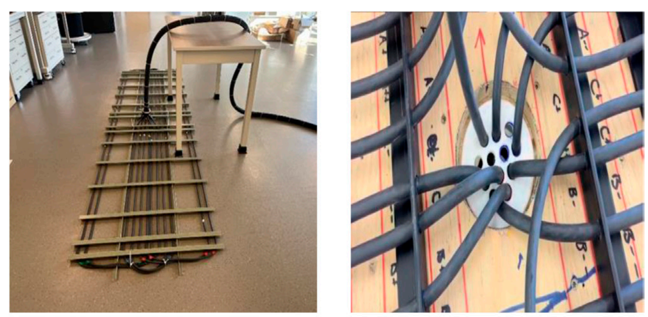

(a) (b)

Figure 4.1 (a) Rail-Rung System and (b) Pattern Plate.

The three-phase tx coils have two turns per phase, requiring 12 individual leads to be routed from the roadway to the roadside power electronics. To manage these connections, the TA utilizes a custom reinforced Printed Circuit Board (PCB) equipped with twelve lever clamps for secure coil interfacing. The PCB internal routing configures the turns of each phase in series and establishes a common neutral point, as illustrated by the dashed lines in Figure 4.3. These connections terminate at banana jacks to provide an interface for impedance characterization. Comprehensive measurements are conducted using a Megger DLR0100H micro-ohmmeter for DC resistance, a B&K Precision 880 handheld LCR-meter for inductance, and a Fluke 375FC ammeter for current verification.

Acceptance testing began with a micro-ohmmeter to verify the DC resistance and magnetic polarity of each winding turn. The ohmmeter is configured for a 10 A excitation current, during which an ammeter is clamped around the turn under test to confirm the correct polarity of the current. Following DC verification, an Inductance-Capacitance-Resistance (LCR) meter is utilized to characterize the AC impedance of the phase and line-to-line inductances. To capture individual phase inductances, the LCR meter is connected between the positive terminal of the phase under test and the common neutral. Line-to-line inductances are obtained by connecting the analyzer across the positive terminals of two respective phases. The final stage of characterization involves measuring line-to-line and turn-to-turn capacitances. These measurements require isolating specific nodes. For line-to-line values, the neutral points (A_{2-}, B_{2-}, C_{2-}) are disconnected from the test fixture, while turn-to-turn capacitances require the negative terminals of all turns to be disconnected. All AC parameters are recorded at 1 kHz, 10 kHz, and 100 kHz to evaluate the frequency-dependent behavior of the coils. This standardized testing sequence allows for the complete characterization of a single tx pad in approximately 15 min.

To establish baseline performance and verify the functionality of the TA, an initial tx coil was evaluated in a laboratory environment prior to roadway deployment. The field evaluation of the 85 tx pads was then conducted across four distinct stages: (i) immediately following coil installation, (ii) after the concrete overlay pour, (iii) subsequent to a winter construction hiatus, and (iv) following final lead termination. Notably, between the post-concrete and post-winter characterizations, the 400-m pilot roadway was opened, exposing the infrastructure to public traffic. Due to an accelerated construction schedule, 69 of the 85 coils were characterized in the pre-concrete stage. The resulting data, summarized in Table 4.1, indicates that the roadway coils generally exhibited higher impedance values than the laboratory prototype. This is primarily attributed to the field leads being approximately 3 m longer than those used in the control.

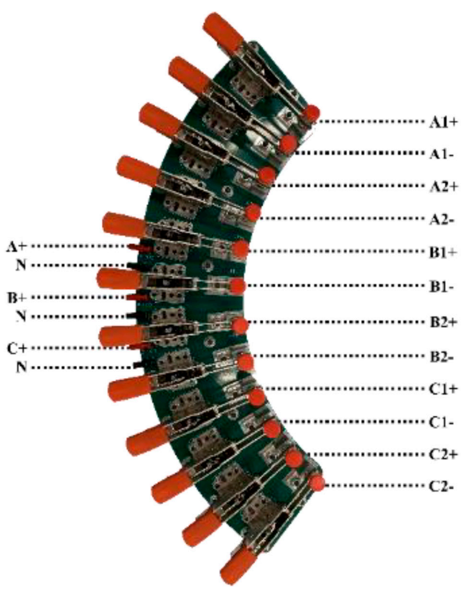

Figure 4.2 Coil Test Apparatus.

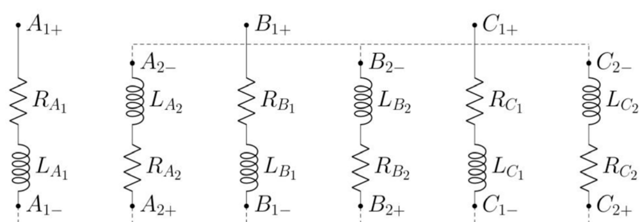

Figure 4.3 Coil Testing Arrangement.

TABLE 4.1
tx Coil Measurements.

Coil Measurement	Lab Prototype	Pre-Concrete	Post-Concrete	Post-Winter	Post-Cut
mean{L^{xy}} (μH)	68	77.59	77.30	77.03	71.19
std {L^{xy}} (μH)	0.42	3.33	3.28	3.00	1.91
mean{L^{11}} (μH)	34.00	38.79	38.65	38.51	35.59
std{L^{11}} (μH)	–	1.64	1.74	1.45	0.92
mean{R^{x}} (mΩ)	36.20	47.56	45.95	42.94	–
std{R^{x}} (mΩ)	0.15	2.70	2.84	2.48	–
mean{TSCF} (%)	0.72	0.98	1.10	1.03	0.77
std{TSCF} (%)	–	0.77	0.99	0.97	0.83

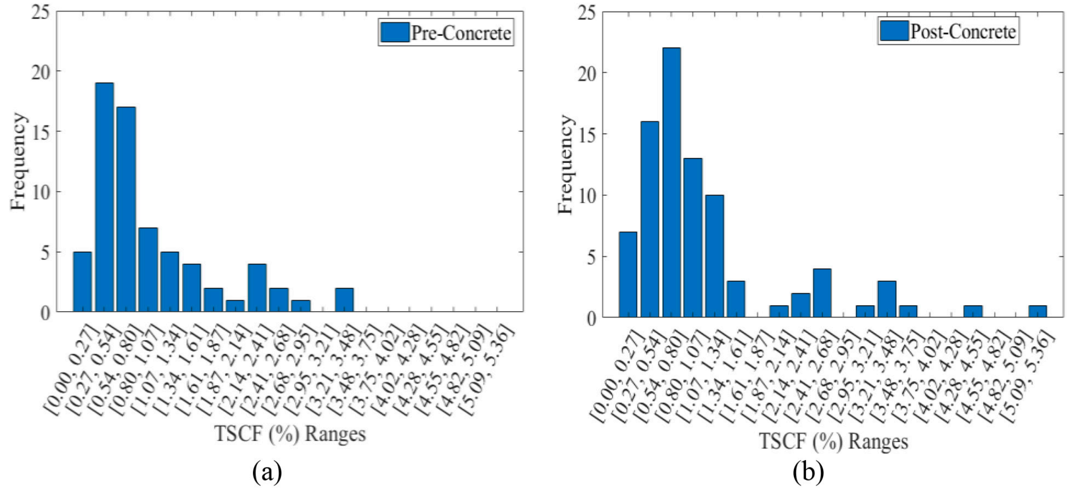

Figure 4.4 (a) TSCF Histograms: Pre-Concrete and (b) TSCF Histograms: Post-Concrete.

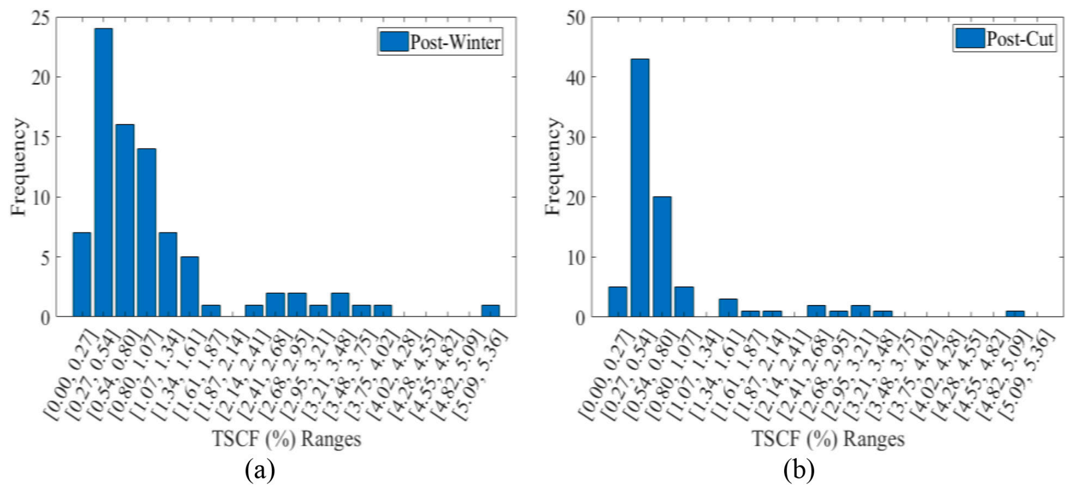

Figure 4.5 (a) TSCF Histograms: Post-Winter and (b) TSCF Histograms: Post-Cut.

Further assessment of the tx coil measurements shown in Figure 4.4 and Figure 4.5 shows the mean TSCF values remained well below the 5% target threshold. The high degree of consistency between the pre-concrete, post-concrete, post-cut, and post-winter measurements indicates that the installation and casting processes were successful and that the electrical integrity of the coils was maintained despite environmental exposure. While the average change in TSCF was negligible, two specific outliers were identified. One coil exceeded the 5% TSCF threshold after the concrete pour, likely due to conductor displacement during the pouring process. Another outlier showed a 3% increase after the winter season, which may be attributed to the unbundling of the twisted leads running from the roadway to the power electronic vaults.

Initial characterizations indicated that the installed inductances were higher than the target values, exacerbated by nonuniform lead lengths. To rectify this, a fourth characterization stage was performed in the spring of 2025 to shorten the twelve individual leads of each coil to a fixed length. This trimming process ensured the tx pads met the TSCF target, as highlighted in Figure 4.5b. This final optimization confirmed that the tx coils were correctly tuned for the system integration and high-efficiency operation despite the lengthy construction process, winter weather conditions, and vehicle loading.

5. MOBILE TEST APPARATUS (MTA) DEVELOPMENT (TASK 3)

To streamline the validation of the 85 inverters that were installed as well as the tx pads, the mobile test apparatus (MTA) underwent two key iterations between late 2024 and 2025. The initial MTA, herein referred to as MTA1, is shown in Figure 5.1 and featured an early-stage receiver (rx) coil, passive rectifier, and compensation circuitry mounted on a wooden chassis. The output of the passive rectifier was tied to a resistive load that was mounted to the deck of the 1,750-lb (payload rated) trailer that was tied to a towing vehicle. The trailer and vehicle are shown in Figure 5.2. Using MTA1, the team brought the trailer

Figure 5.1 MTA1, Which Was Manually Placed Over a Transmitter Pad, During Testing.

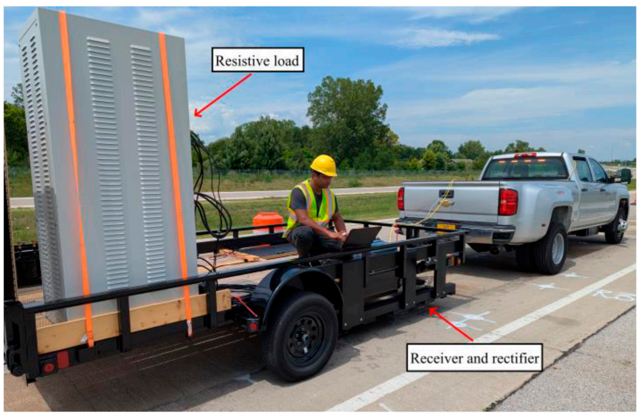

Figure 5.2 MTA2, Where the Receiver Is Mounted on the Underside of the Trailer.

to the roadway, unloaded it and placed it over a corresponding transmitter coil for stationary testing. The stationary testing was used to both ensure the system operated as expected and to perform acceptance testing of the inverters.

To improve testing efficiency and reduce setup time, a second revision of the MTA, referred to as MTA2, integrated the rx coil and electrical components directly beneath the trailer, as seen in Figure 5.2. The MTA2 configuration proved to be highly effective, facilitating both unregulated stationary and dynamic testing of the DWPT system throughout the fall of 2025. These successful trials served as the final preparation for upcoming roadway testing with the Cummins vehicle.

6. SUPPORTING DWPTT ACCEPTANCE TESTING (TASK 4)

Roadway testing validated that the electrified roadway and vehicle can reliably “hand off” power from pad to pad while a receiver moves down the corridor. Validation was executed in four escalating phases: (1) unregulated stationary tests to confirm each transmitter–inverter pair operates correctly at low and then higher power, (2) unregulated dynamic tests to verify that the roadway can detect a moving receiver and properly activate downstream pads in time, (3) regulated stationary tests to confirm commanded-power regulation with the vehicle’s DC–DC converter near the system’s upper capability, and (4) regulated dynamic tests to demonstrate high-power transfer at highway speeds.

In the first phase, a validation that the transmitter-receiver pairs were sending/receiving power served to provide acceptance testing of each inverter. During early Phase 1 testing, MTA1 was hand-placed over each of the transmitters and the resistive load at the output of the receiver rectifier was configured to dissipate power at specified levels. A detailed description of the validation and characterization results of the Phase 1 hardware testing is provided in a later section of the report. As an example of the behavior observed, the tx and rx currents and output power level measured are shown, along with values predicted from simulations used in the design process, in Figure 6.1 through Figure 6.3, respectively.

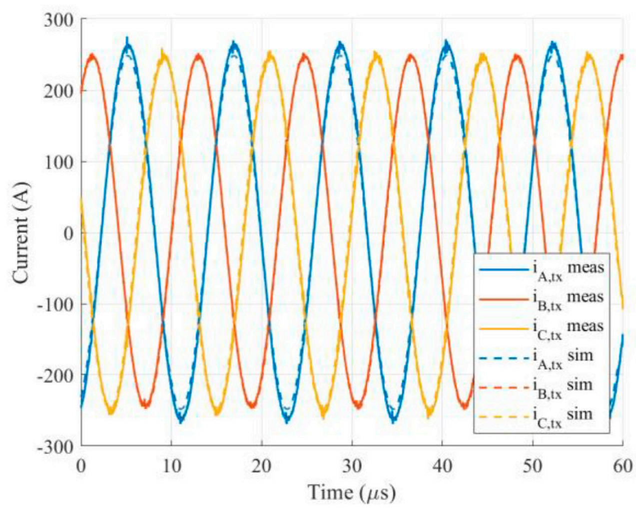

Figure 6.1 Experimental Measurements of Transmitter Currents Overlaid With Simulated Data.

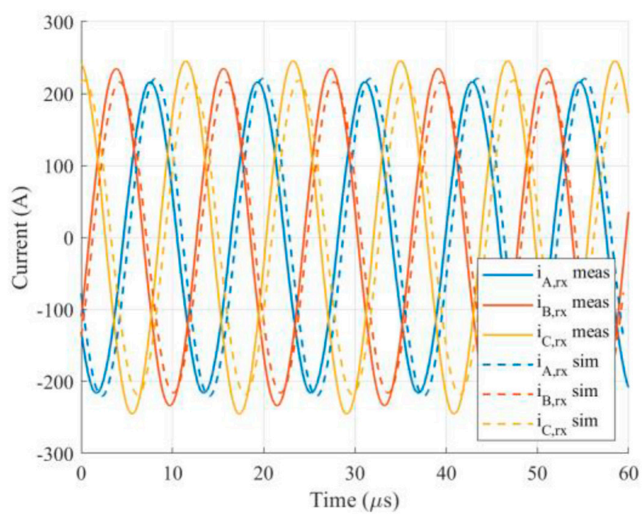

Figure 6.2 Experimental Measurements of Receiver Currents Overlaid With Simulated Data.

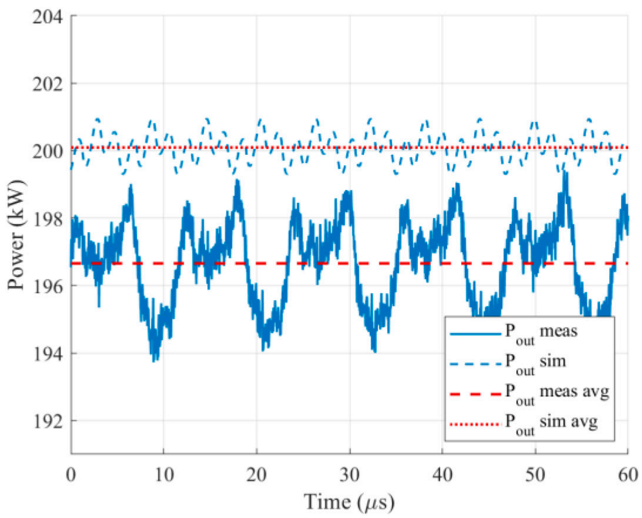

Figure 6.3 Experimental Measurements of Rectified Power Overlaid With Simulated Data.

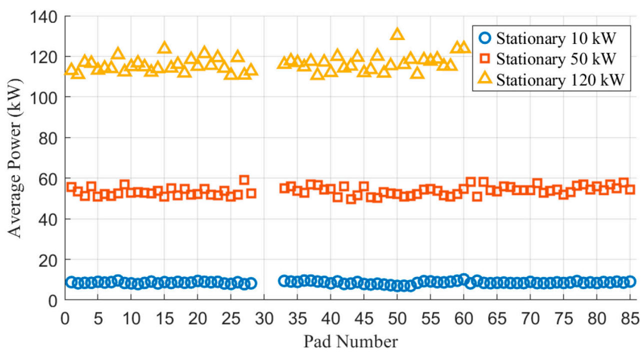

Figure 6.4 The Average rx Power for Each tx.

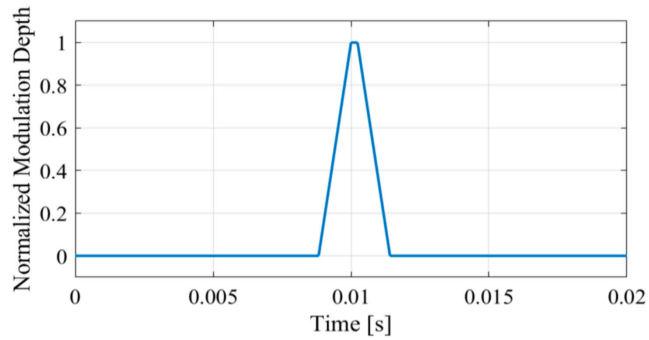

Figure 6.5 Illustrative Example of the Vehicle-Capture Pulse Train Used for Inverter Controls.

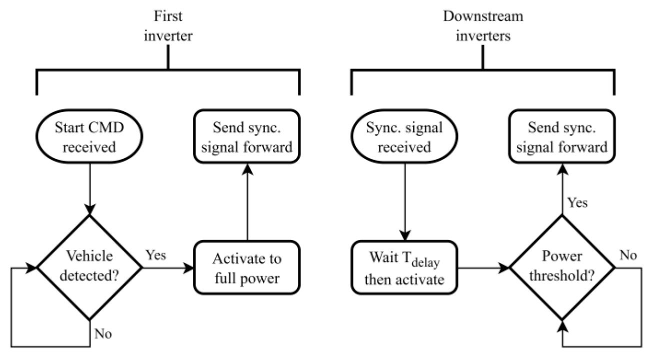

Figure 6.6 Flowchart of the Inverter Vehicle-Detection and Forward-Synchronization Logic.

The data from the early Phase 1 testing validated that the roadway hardware was capable of providing wireless power transfer on the order of 200 kW and matched expected performance. A second takeaway from the testing was that imbalance on the receiver currents was slightly higher than predicted from simulation, which was likely caused by misalignment between the tx–rx pair. This imbalance tended to yield an insignificant increase in the observed rectified power ripple.

Testing a transmitter/inverter utilizing MTA1 required on the order of 10–15 min as it was a manually intensive process. As Phase 1 testing continued, MTA2 was leveraged wherein the rx coil was mounted to the underside of a trailer and towed by a pickup truck. This allowed for validation of power delivery at a wide range of power levels (10 kW, 50 kW, and 120 kW). The receiver output power obtained during this stage of Phase 1 testing is shown in Figure 6.4. As observed in Figure 6.4, the measured output power at all testing levels had minimal variation across tx pads. Coupled with the TSCF measurements acquired during initial characterization, these results validated that the roadway infrastructure and associated P.C. Krause and Associates inverters conformed to their design specifications. It is noted that pads 29–32 were excluded from the Phase 2 stationary testing due to repairs that were required for Inverter #30. Inverter #30 was damaged during the early stages of Phase 1 stationary testing when it was placed under a load exceeding its rating. It is further noted that the later stages of Phase 1 testing were performed up to 120 kW. Further higher power testing was limited to meet project scheduling constraints.

Prior to describing Phase 2 dynamic testing, it is convenient to describe the inverter triggering/synchronization utilized. The inverters were configured to utilize a vehicle-detection and synchronization scheme wherein each inverter sends short, low-duty "detection" pulses (Figure 6.5) and monitors its input power; if the pulse power exceeds a threshold, the inverter declares the vehicle is present and transitions into full DWPT operation. Once a leading inverter captures the vehicle, it triggers downstream inverters (with a fixed delay used during at-speed testing) so that only pads under/just ahead of the vehicle are energized and phase-aligned along the corridor. Figure 6.6 outlines this simple state-flow for each type of inverter (leader or follower). Figure 6.7 displays a real-world example of an inverter's vehicle detection algorithm finding a vehicle and fully energizing its transmitter pad.

In Phase 2 unregulated dynamic testing, MTA2 was utilized wherein receiver power was provided to a resistive load. To account for potential construction imperfections and

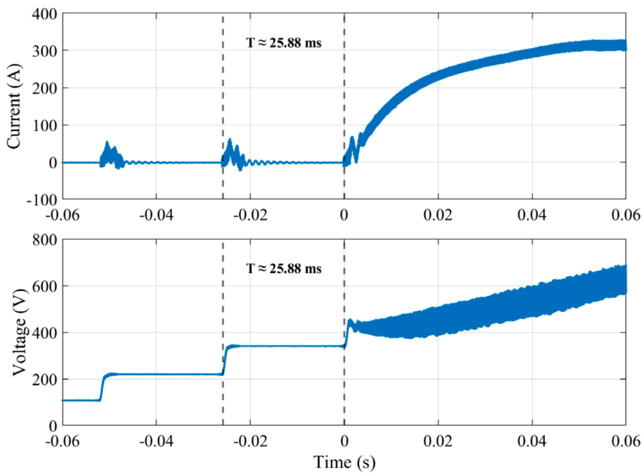

Figure 6.7 Measured Inverter Input Current and Receiver Output Voltage Response During a Vehicle Detection Event.

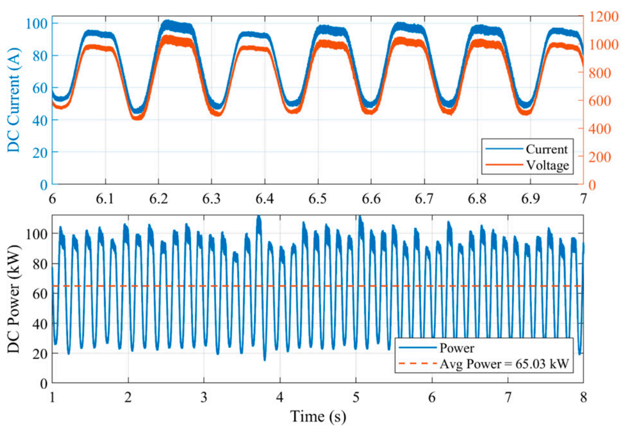

Figure 6.8 Measured rx-Side Power Obtained During Phase 3 Dynamic Testing With MTA2.

misalignment, the load resistance used during unregulated dynamic testing was set to draw 100 kW from the roadway. Testing commenced at 30 mph and successfully scaled to 65 mph. The measured rx power waveforms were highly consistent across the entire 84 tx pads (coil 30 was not utilized), which demonstrated the robustness of the synchronization logic and overall readiness of the pilot project infrastructure for highway-speed heavy-duty vehicle charging. A representative set of data obtained across a 30-pad stretch is shown in Figure 6.8.

The results show successful multipad power transfer at highway speed. In unregulated dynamic testing, the system achieved clear pad-to-pad "chain" operation but with some power fluctuation (e.g., ~65 kW average and ~113 kW peak at ~65 mph), consistent with the fact that a fixed resistive load cannot regulate through voltage variations that occur during pad transitions and misalignment. The Phase 3 and Phase 4 dynamic regulated testing with the Cummins vehicle is outlined in Task 5 (Chapter 7) alongside grid to vehicle efficiency metrics.

7. VEHICLE ASSEMBLY AND TEST (TASK 5)

To enable wireless power transfer for the Cummins Class-8 EV, Purdue University developed the key receiver-side components: the DWPT receiver and the onboard DC–DC converter. These components were codesigned with Cummins to ensure seamless vehicle integration and roadway readiness. The Purdue–Cummins teams met biweekly throughout 2024–2025 to finalize the designs and closely track build progress and validation.

7.1 DC–DC Converter

The DC–DC converter is a critical component of the DWPT system because it enables safe, controlled power transfer. It bridges the voltage gap between the highly variable receiver voltage (caused by changes in tx–rx coupling) and the relatively stable vehicle battery voltage. Installed between the receiver and the vehicle battery, the converter regulates power flow to the vehicle. An interleaved buck-boost converter topology, as shown in Figure 7.1, is used to provide this voltage-bridging capability and enable DWPT power control. The converter can operate in either buck or boost mode, providing power control when the receiver voltage is lower than or higher than the battery voltage, respectively. As a result, it can maintain power delivery even under vehicle misalignment.

The DC–DC converter was designed and developed at Purdue to handle 200 kW of DWPT power to the vehicle. Figure 7.2 shows the DC–DC converter hardware, featuring four Wolfspeed CAB320M17XM3 SiC modules mounted on a high-current PCB bus bar. The power modules are driven by CGD1700HB2P-XM3

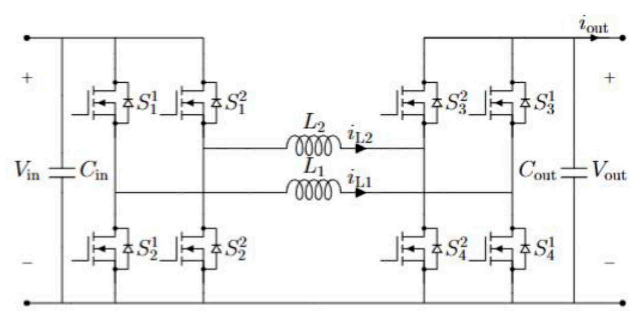

Figure 7.1 DC–DC Converter Topology.

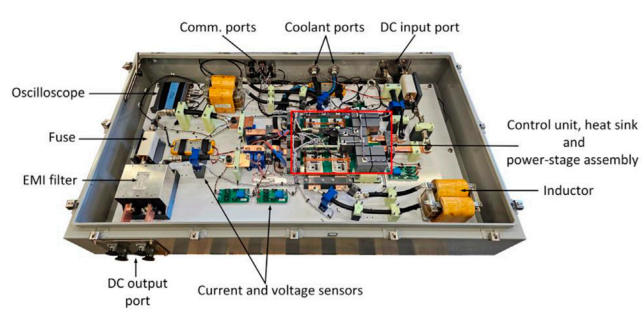

Figure 7.2 200-kW Onboard DC–DC Converter and its Components.

gate drivers, which also provide fault monitoring and Pulse Width Modulation (PWM) feedback to track device temperature, essential for safe operation. A contactor system precharges the output capacitor from the vehicle battery, isolates the system during faults, and is backed by high-current fuses for short-circuit protection. The SiC modules are mounted on a heat sink, connected to a coolant line pumping 50/50 glycol-water mix. Additionally, the system includes allocated space for an output EMI/EMC filter to mitigate common-mode noise.

The control logic is implemented on a TI C2000 F28388D dual-core micro-controller, mounted on a custom PCB powered by a 24-V supply. The system uses LEM 505-S and LEM LV 25-1000 sensors for the current and voltage feedback, respectively. Communication with the truck is facilitated through a 500-kbps CAN (Controller Area Network) bus. Both the vehicle supervisory control module (SCM) and the converter feature high-side drivers, ensuring a redundant mechanism to induce safe shutdown in case of communication failure. CRC (cyclic redundancy check) and rolling counters are used for communication fault detection. A state-flow model complements the control logic to manage operations like sensor calibration and precharging. This event-driven approach ensures reliable converter control via the SCM. To ensure the system is weatherproof, the converter is mounted on an aluminum base plate and enclosed in a waterproof steel case. The input and output connections are made through IP67-rated power connectors, while the 24-V power and low-level logic signals use other waterproof connectors.

To validate full-power (200 kW) operation and integration with the vehicle-side controller, the converter was then evaluated at Cummins's high-power EV laboratory. Rigorous high-power hardware-in-the-loop testing was conducted to emulate near real-world operating scenarios, including DWPT roadway behavior across multiple vehicle speeds. This laboratory campaign was critical for demonstrating converter reliability, system integration, and control performance. The resulting feedback informed improvements to both the mechanical implementation and the control strategy. The device was isolated in a test cell, as shown in Figure 7.3 where it was remotely controlled and monitored via CAN bus integrated using AVL Puma and Lynx test automation systems located in a separate control room. The converter was powered by a 250-kW power supply operating in voltage control mode. A pump maintained the temperature and flow rate of the coolant to the heat sinks at 60 °C and 15 L/min (at 24 psi), emulating the worst-case scenario possible in the EV.

First, to validate that the hardware performs as expected, the converter was tested under multiple loads. Figure 7.4 and Figure 7.5 illustrate the converter response when a high-power step reference is applied in buck and boost mode, respectively. The converter output power stabilizes at the referenced value in under 25 ms. Then, to evaluate performance under emulated real-world scenarios, the converter was tested with varying input voltage at multiple loading points. The input voltage profile was generated to emulate a vehicle traveling over the DWPT roadway. Figure 7.6 illustrates a variable-voltage test in a partially loaded condition. The converter is given a 50-kW command while the input voltage profile varies between 300 V and 750 V, emulating a vehicle moving at 50 mph with full tx–rx

Figure 7.3 Converter in Test Cell.

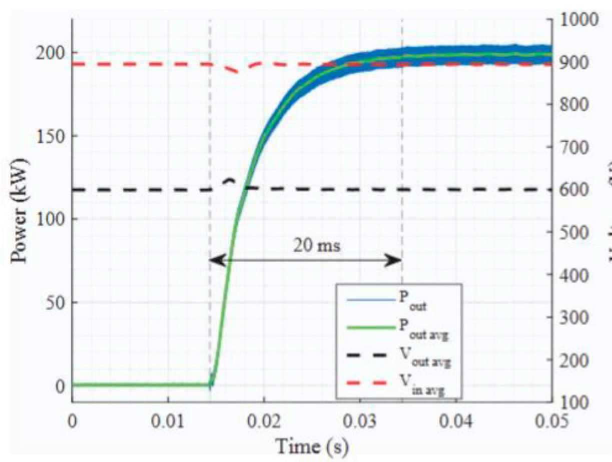

Figure 7.4 200-kW Test in Buck Mode.

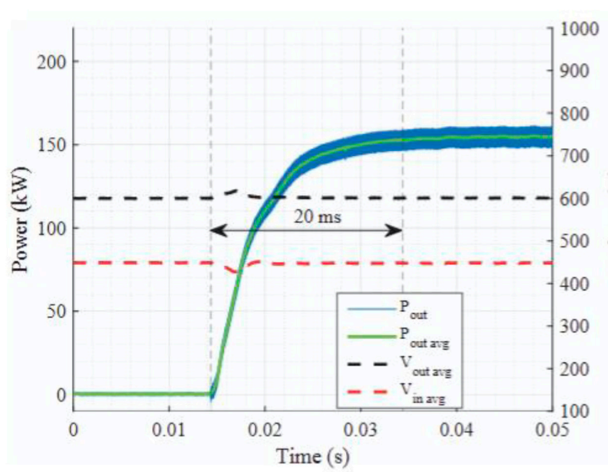

Figure 7.5 150-kW Test in Boost Mode.

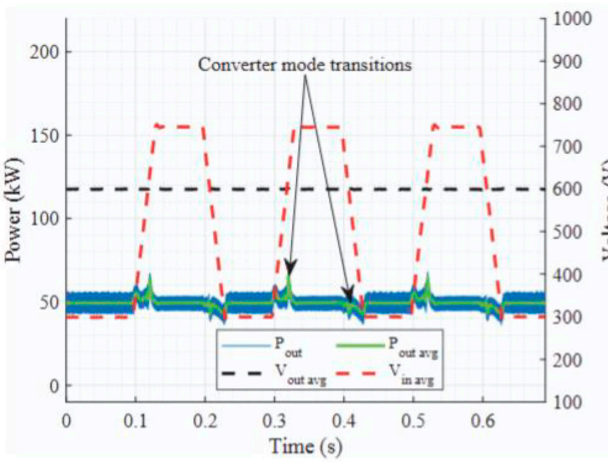

Figure 7.6 50-kW Test with Variable Input Voltage at 50 mph.

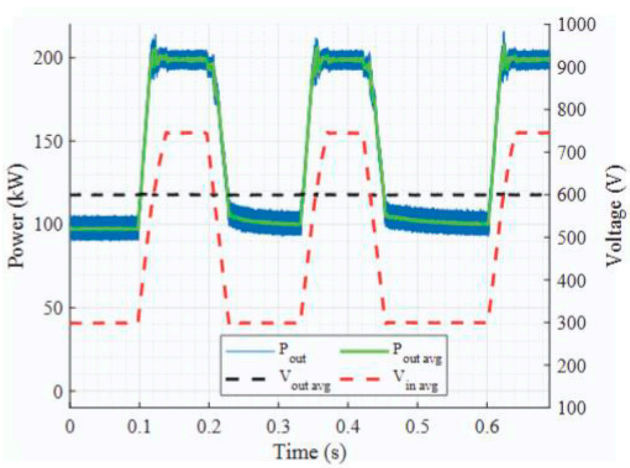

Figure 7.7 200-kW Test With Variable Input Voltage at 50 mph.

lateral alignment. The output voltage is kept constant at 600 V throughout the test. It can be seen in Figure 7.6 that the output power is regulated well at 50 kW.

Figure 7.7 illustrates the converter operation with variable input voltage at a commanded power of 200 kW. At low input voltage, the power output saturates at 100 kW, limited by the converter current rating. As the voltage rises, it can be seen that the power follows the input voltage profile, and then it is regulated at 200 kW as soon as sufficient input voltage is available. If the power command exceeds the converter capability for a given input voltage, the controller drives the inductor current to its maximum (180 A). This functionality drives the converter to its maximum power capability, enhancing system utilization under tx–rx misalignment. The converter achieved efficiencies between 97% and 98.5%, depending on the operating mode and loading conditions. During a 200-kW test of one minute (Vin = 750 V, Vout = 600 V) with initial MOSFET temperatures at 56 °C, the peak temperature reached only 64 °C, confirming the thermal stability of the converter. Testing at the Cummins facility was formally completed in April 2025, and a conference paper detailing the DC–DC converter and its operation has been published in the Wireless Power Transfer Conference and Expo (WPTCE), 2025, Rome, Italy (Mehar et al., 2025).

7.2 Receiver Coil Assembly

The receiver assembly that is placed at the underside of the Cummins truck and ties to the DC–DC converter was also designed at Purdue. The assembly includes three important components: the DWPT receiver coil, the receiver-side compensation circuit, and the AC–DC three-phase rectifier. These components were assembled within a nonmagnetic plastic case and were covered using an aluminum shield to protect the vehicle and its components from stray magnetic fields. Figure 7.8 illustrates the receiver assembly and its constituent components. The receiver coil is housed under the aluminum shield and receives the magnetic flux emanating from the transmitter coil. The time-varying flux generates a voltage across the receiver coils when the vehicle is over a transmitter. The compensation circuit consists of a three-phase capacitor network connected in series with the three-phase rx coils. It tunes the system to a given operating frequency and helps generate a load-independent output voltage at the receiver terminals. The AC receiver voltage is converted to a DC voltage source using the three-phase rectifier and is provided to the DC–DC converter.

7.3 Electrical Roadway Testing

The system testing with the Cummins vehicle, which represented Phase 3 and 4 of the roadway testing performed, began on the roadway in October 2025. The DC–DC converter and receiver assembly were integrated with the Cummins vehicle as shown in Figure 7.9. The DC–DC converter was connected

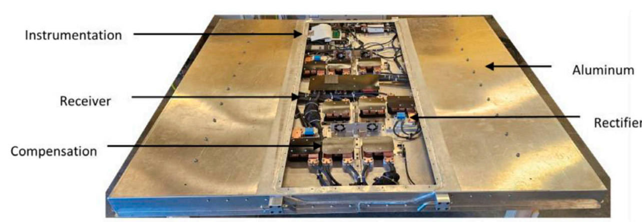

Figure 7.8 Receiver Assembly and Its Components.

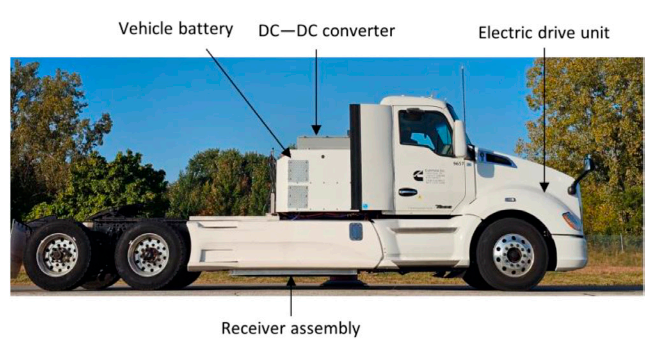

Figure 7.9 DWPT-Enabled Cummins Class-8 EV.

to the DC-link that serves the vehicle battery pack and traction inverter. The input to the DC–DC converter is connected to the output of a six-pulse passive rectifier that is tied to the rx coil.

7.3.1.1 Phase 3: Static Tests with Cummins Vehicle. To verify system operation, several static power-transfer tests were conducted with the truck parked over a single roadway tx pad. In each static test, one tx pad was energized while the truck commanded constant power through the DC–DC converter. Figure 7.10 presents measured results from a 180-kW static power-transfer test. As shown, the rx output DC voltage increases as the inverter ramps current in the tx coil. The output power is regulated at 180 kW, confirming effective power control.

As intended, the tx inverter includes a 500 ms on-time limit. Once the inverter shuts down at this limit, the DC–DC converter continues operating by drawing energy from its input capacitor bank until the input voltage drops below the converter cutoff threshold. At that point, the power transfer to the DC-bus stops. Figure 7.11 shows a zoomed view of the converter turn-on transient. The converter begins operating when the input voltage reaches 400 V, after which the output current ramps to its commanded level. Additional tests were performed with the truck positioned over different pads and with varying tx–rx overlap conditions to confirm nominal system performance.

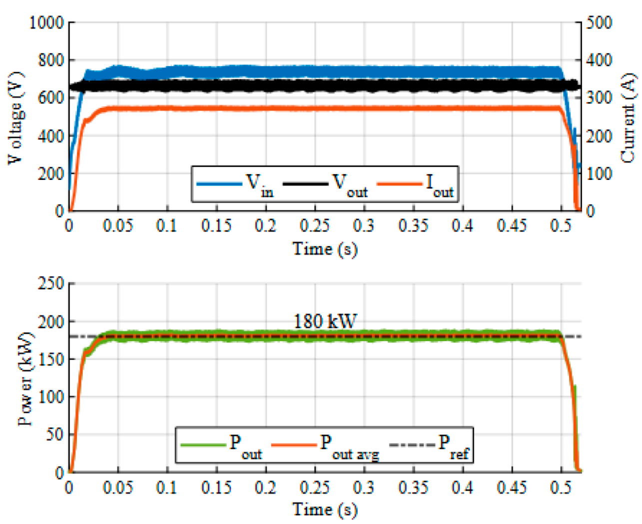

Figure 7.10 180-kW Static Test.

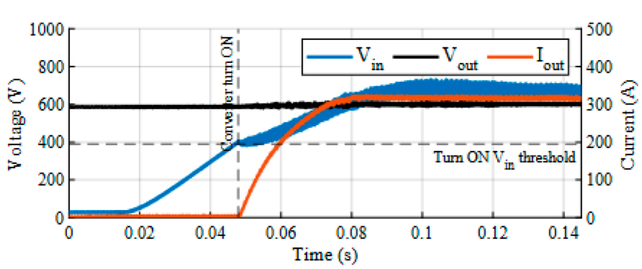

Figure 7.11 DC–DC Converter Startup Transition.

7.3.1.2 Phase 4: Dynamic Test with Cummins Vehicle. In dynamic tests, the vehicle was driven over the electrified roadway at fixed speeds while the SCM commanded power to the DC–DC converter. Figure 7.12 shows converter performance at a 50-kW power command and 65-mph vehicle speed. The roadway results closely match the hardware test-bench results. The measured input voltage waveform has a trapezoidal shape as the vehicle passes over multiple tx pads. Unlike the lab setup, however, waveform crest and trough levels vary from pad to pad due to practical nonidealities, including lateral and vertical tx–rx misalignment, tx inductance variation, and roadway surface unevenness. The battery voltage remains relatively constant during the test.

Figure 7.13 shows converter response to a 150-kW command at 65 mph. As the vehicle moves across successive tx pads, the output power follows a trapezoidal profile, reaching the commanded

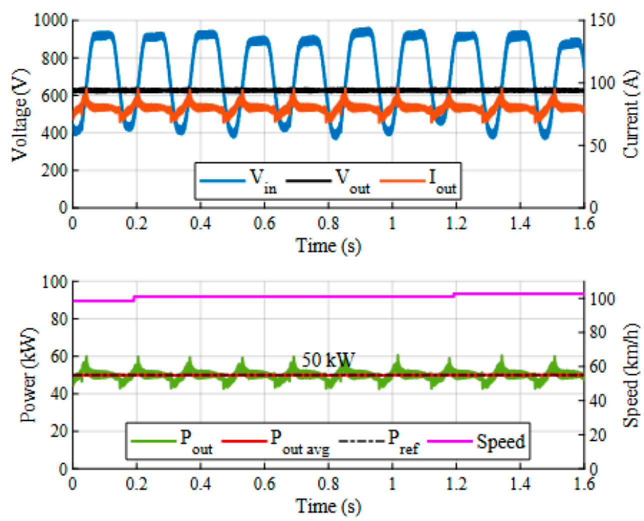

Figure 7.12 50-kW Dynamic Test at 65 mph.

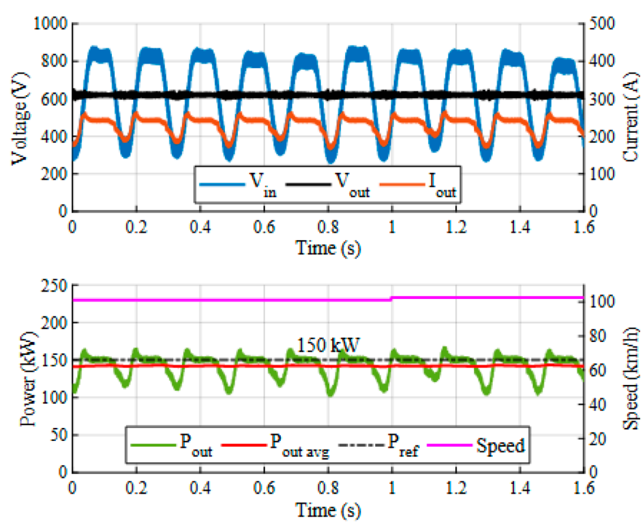

Figure 7.13 150-kW Dynamic Test at 65 mph.

150 kW during full tx–tx overlap and dropping to about 100 kW during pad transitions. The average delivered power is close to the reference power, and the converter transitions smoothly between buck and boost modes. Figure 7.14 shows similar behavior for a 190-kW command at 65 mph. Power is regulated at 190 kW during full overlap and falls to about 100 kW between pads, yielding an average output of about 170 kW. Although laboratory testing reached the 200-kW rated level, roadway testing was limited by the battery-based DC input supply.

In November 2025, the conference publication was invited for extension as a journal article in the *IEEE Journal of Wireless Power Technologies*. The extended manuscript presents the DC–DC converter design and operation in substantially greater detail and includes roadway testing results that validate the real-world performance of the implemented solutions. The journal manuscript has been submitted and is currently under peer review. Arguably one of the most important metrics for this technology is the grid-to-battery efficiency. Due to lack of probing capable of measuring true grid efficiency, Figure 7.15 shows the inverter input to vehicle battery efficiency for a representative 190-kW test at 84.51%. This is within the current Society of Automotive Engineers (SAE) standards for stationary wireless power transfer.

Looking ahead, Purdue will continue analysis and targeted testing to further quantify system performance and inform future design iterations. Several conference and journal manuscripts are currently in development that document the underlying design rationale, modeling assumptions, and analytical methods in greater technical depth. In the coming months, additional measurements will address data gaps from earlier campaigns, including end-to-end grid-to-battery efficiency, misalignment sensitivity and operating margins (lateral/longitudinal/vertical), and a comprehensive loss characterization across power levels and speeds (roadway power electronics, magnetic link, and vehicle-side conversion). These efforts will strengthen the technical basis for standardization discussions and provide the performance evidence needed to support broader deployment planning.

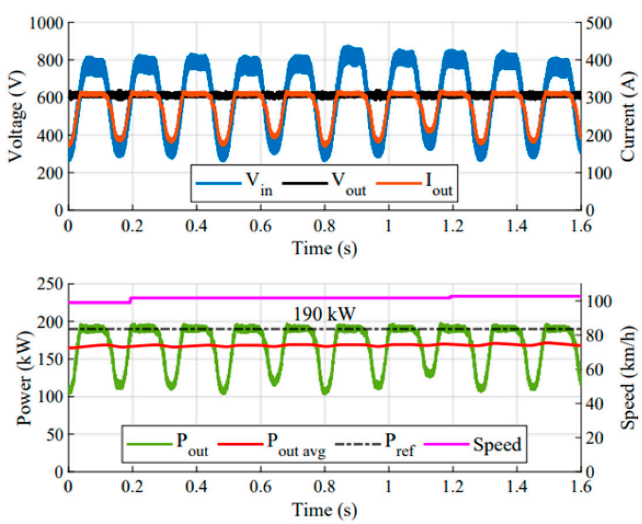

Figure 7.14 190-kW Roadway Testing at 65 mph.

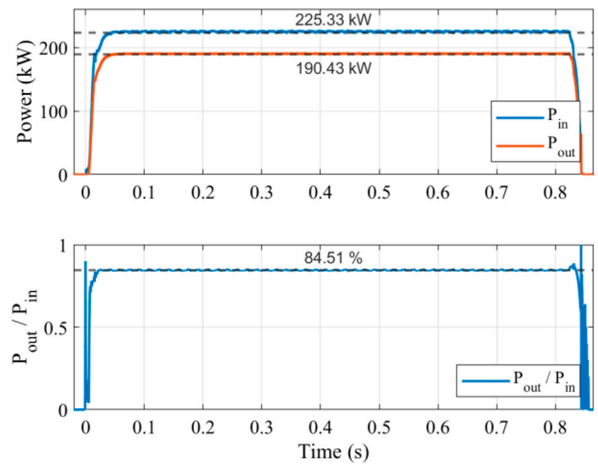

Figure 7.15 Vehicle Power Waveforms During a 190-kW Regulated Dynamic Test at 65 mph.

8. COMMUNITY OUTREACH (TASK 6)

This chapter provides an overview of the community engagement and research activities conducted as part of the Indiana Department of Transportation (INDOT) DWPT pilot project. Beginning in late June 2024, the project team collaborated with INDOT to design and distribute a public feedback survey to gather initial community perspectives. In September 2024, the team hosted a public open house to inform community members about the DWPT project and to directly engage with stakeholders regarding their questions and concerns. Following the open house, survey data were cleaned and analyzed using a mixed-methods approach, drawing on responses from 275 participants. The findings from this analysis informed the development of a research paper, which was presented at the 2026 Transportation Research Board Annual Meeting to disseminate results and solicit feedback from transportation researchers and practitioners. Given the limited existing literature on public perceptions of DWPT, this work serves as a pilot study aimed at identifying perceived benefits, concerns, and considerations related to the deployment of this technology.

8.1 Survey Design and Data Collection

8.1.1 Survey Design

The research team designed a stated preference survey to study how the public views the DWPT pilot, EVs, and charging options. The survey included both open-ended and closed-ended questions and was paired with a mixed-methods analytical approach. The qualitative content analysis of open-ended comments helped identify new themes, clarified what people perceived as benefits and concerns, and provided context for differences found in the quantitative data. The quantitative analysis measured how prevalent certain respondents' views were and examined the relationships among them. Combining insights from both methods strengthened the validity of the study's conclusions. It also produced more accurate recommendations for local electrification policy and public education outreach.

8.1.2 Survey Data Collection

The questionnaire, hosted online, circulated through social media, press releases, and the project website (INDOT, 2024). The respondents were able to participate between June and September 2024, during testbed construction. We chose to include all respondents who self-identified as residents of Indiana, not just Greater Lafayette, due to the nature of college towns: many students, faculty, and staff who work or attend school in West Lafayette may live in other parts of the state or move throughout the year. These individuals may not identify as Lafayette residents but are affected by the DWPT testbed, nonetheless.

8.1.3 Sample Description

At the beginning of the survey, two screening questions were included to ensure that the participants were (i) adults and (ii) living in Indiana. The survey also included two attention checks to ensure that respondents read the survey carefully and conscientiously answered the questions. These questions asked the participants to select a specific option in closed-ended questions. The median time of the respondents who completed the survey was calculated, and the respondents who finished in less than one-third of this time were excluded from the final sample. In view of these criteria, from the 455 respondents who started to answer the survey, a sample size total of 275 valid participants is considered in this study. Particularly in the qualitative analysis, the responses of only 134 participants were analyzed as the other respondents did not provide any additional comments to the survey when asked in the open-ended question. Figure 8.1 illustrates the data cleaning procedure.

8.1.4 Socio-Demographic Information

Males represent approximately 55% of the total sample, while the total number of females is slightly lower than 40% of the total. Regarding age, more than 50% of respondents are in the range between 35 to 55 years old, as illustrated by Table 8.1, which displays the age and gender composition of the survey sample.

TABLE 8.1
Age and Gender Distribution.

	Male	Female	Other/Prefer Not to Say
18–24 Years Old	13 (4.7%)	5 (1.8%)	1 (0.4%)
25–34 Years Old	38 (13.8%)	20 (7.3%)	7 (2.5%)
35–44 Years Old	32 (11.6%)	22 (8.0%)	3 (1.1%)
45–54 Years Old	27 (9.8%)	28 (10.2%)	1 (0.4%)
55–64 Years Old	17 (6.2%)	11 (4.0%)	2 (0.7%)
Over 65 Years Old	24 (8.7%)	17 (6.2%)	0 (0.0%)
Prefer Not to Say	0 (0.0%)	1 (0.4%)	6 (2.2%)
Total	151 (54.9%)	104 (37.8%)	20 (7.3%)

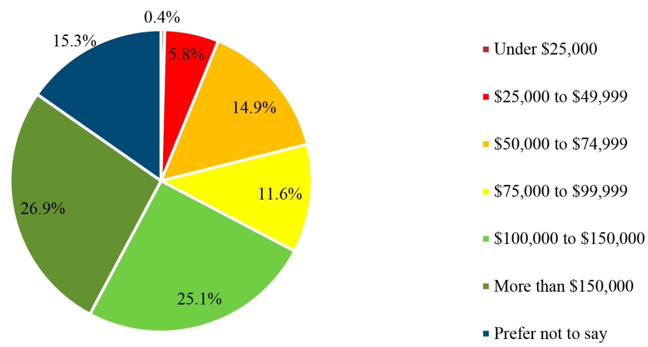

Figure 8.2 Survey Sample Household Income Distribution.

Regarding household income, most of the respondents earn more than $100,000 annually, with approximately a quarter receiving more than $150,000. Figure 8.2 shows the household income distribution of the sample.

8.1.5 Experience with EVs

Participants were also asked about their experience with EVs. Approximately a quarter of the sample currently own or lease an EV, and more than half of the total number of respondents

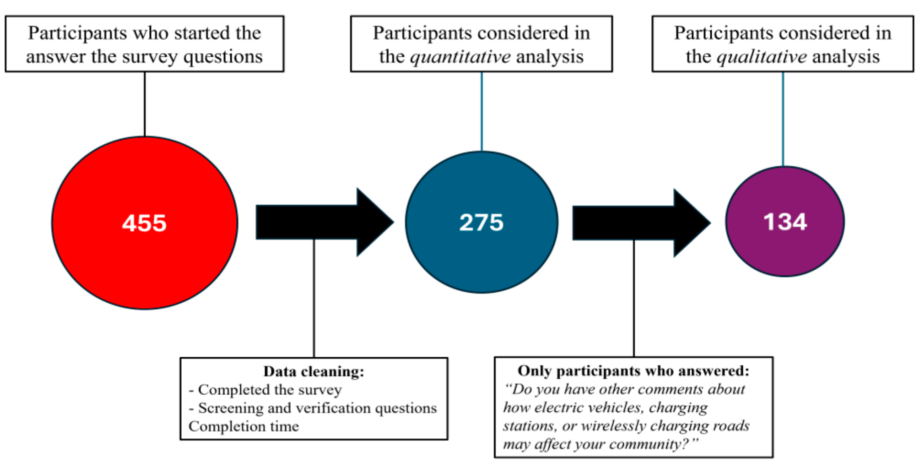

Figure 8.1 Data Cleaning Procedure for the Sample.

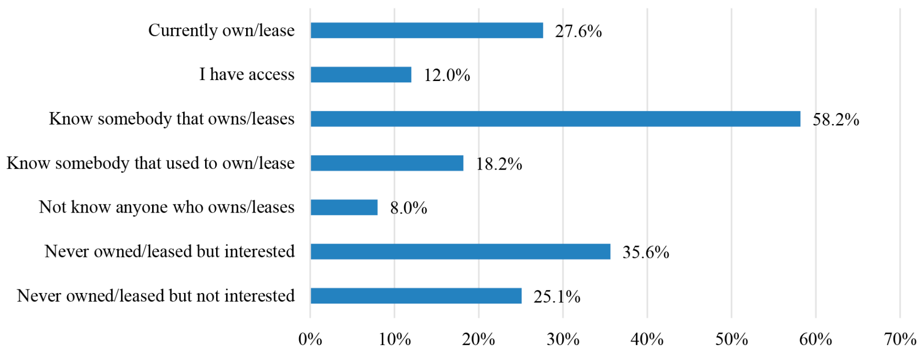

Figure 8.3 Survey Sample Experience with EVs.

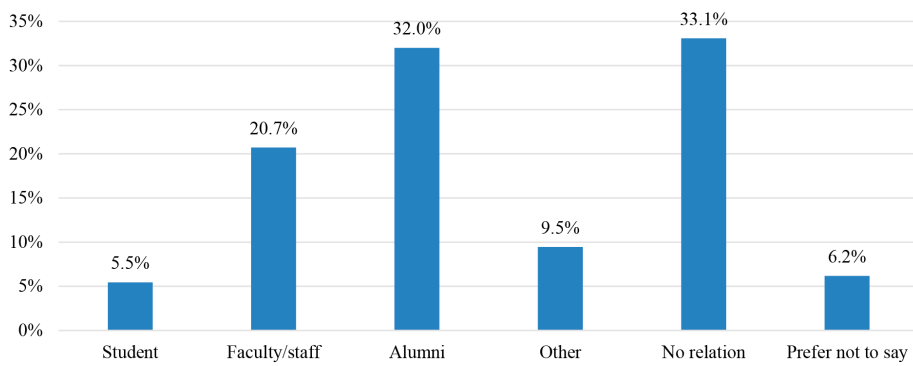

Figure 8.4 Survey Sample Relationship with Purdue University.

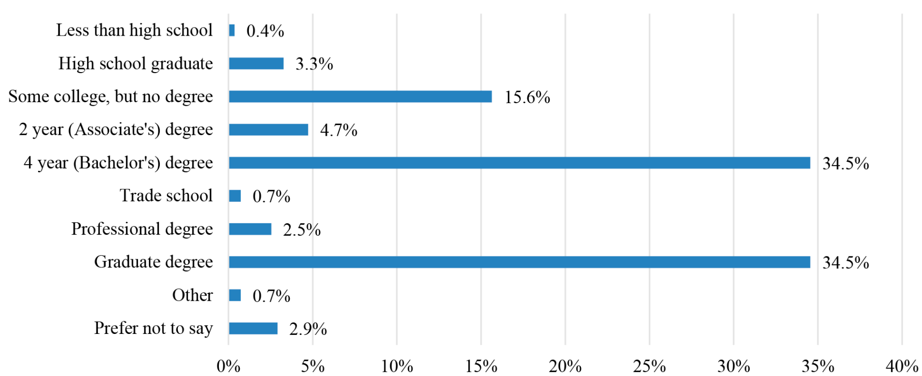

Figure 8.5 Survey Sample Educational Level.

know someone who owns or leases these vehicles. Additionally, approximately a third of the sample stated that they have never owned or leased an EV but are interested in one. Figure 8.3 shows the experience with EVs of the participants.

8.1.6 Relationship with Purdue University

As the testbed is located in Greater Lafayette, an area where many inhabitants have a connection with Purdue University, participants were also asked about their relationship with the institution. Approximately one-third of the sample has no relationship with it, while another third part are Purdue Alumni. The remaining are split between faculty/staff, students, and others. Respondents were able to select multiple options (example: Faculty and Alumni). Figure 8.4 presents the whole distribution of the participants.

8.1.7 Educational Level

Regarding educational level, more than half of the participants have some type of degree. Specifically, a third have graduate degrees, while another third of the participants have a bachelor's degree as their highest degree attained. Figure 8.5 shows the educational level of all participants.

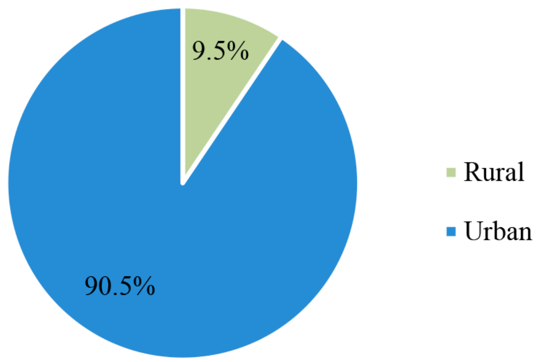

Figure 8.6 Survey Sample Home Location.

8.1.8 Home Location

Respondents provided the ZIP code of their home location. Rural-Urban Commuting Area (RUCA) codes were used to classify participants' home location as rural or urban. Approximately 90% of the participants live in urban areas, as illustrated by Figure 8.6.

8.2 Survey Data Analysis (Task 6)

8.2.1 Quantitative Results

8.2.1.1 Knowledge of Transportation Electrification. The survey participants were also asked about their knowledge regarding the different types of vehicles in transportation electrification. Figure 8.7 shows that all different types of analyzed vehicles are recognized by the participants, with EVs being the most familiar one, as approximately one-third of the sample stated to know a lot about them. Figure 8.8 displays the participants' familiarity with charging technologies. Level 1 and Level 2 have similar levels of familiarity, while the DWPT is the least familiar technology for the participants. Participants were also asked about their knowledge of the INDOT DWPT Testbed, as shown in Figure 8.9. More than 90% of the sample stated to know or have heard about the project, although the level of knowledge is not deep, as less than 10% stated to know a lot about it.

8.2.1.2 Concerns with Transportation Electrification. The main concerns with the DWPT technology were examined

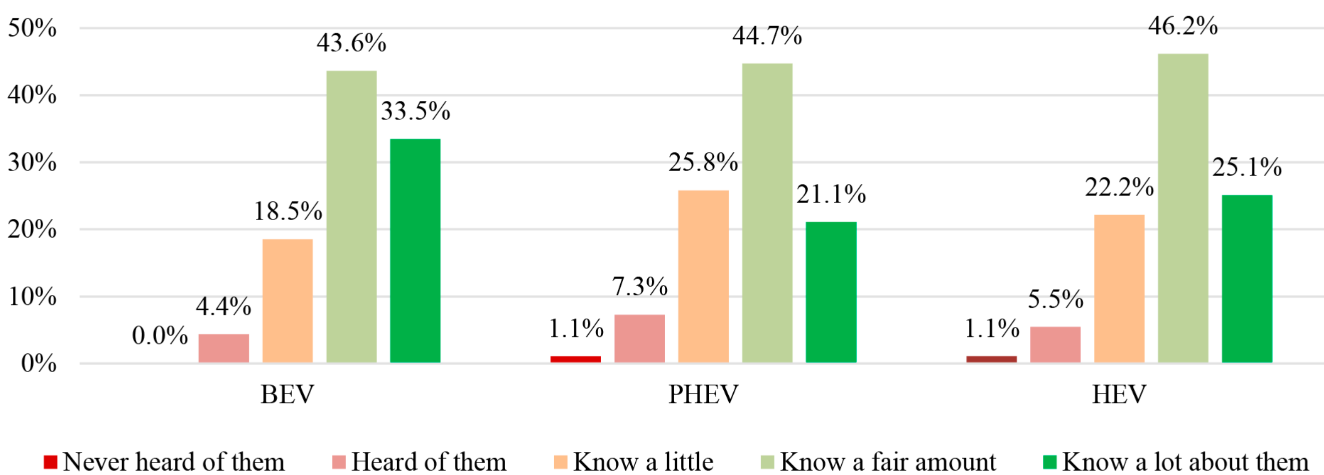

Figure 8.7 Participants' Knowledge of EVs, Plug-in Hybrid Electric Vehicles (PHEVs), and Hybrid Electric Vehicles (HEVs).

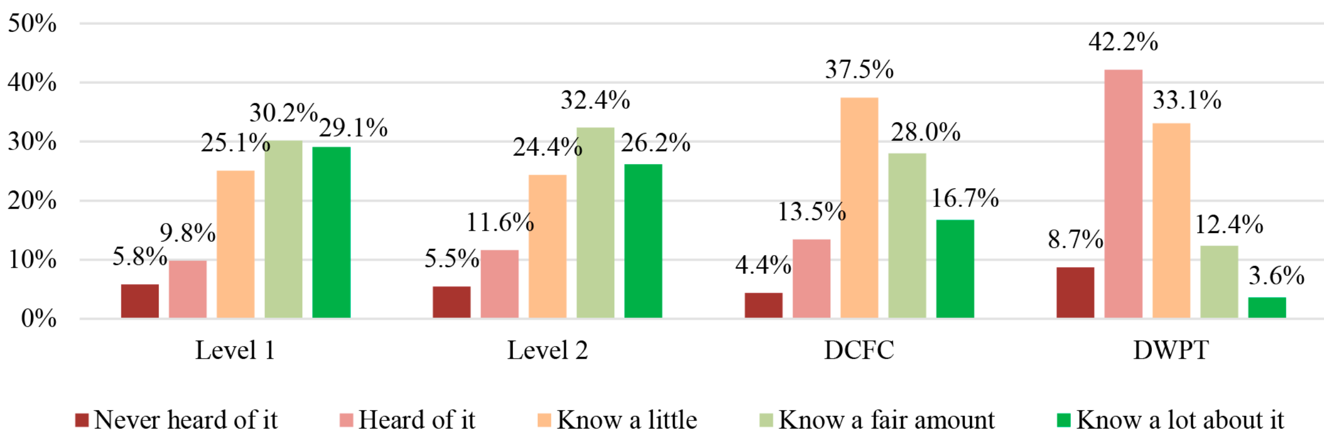

Figure 8.8 Participants' Knowledge of Charging Technologies Familiarity With INDOT DWPT Testbed.

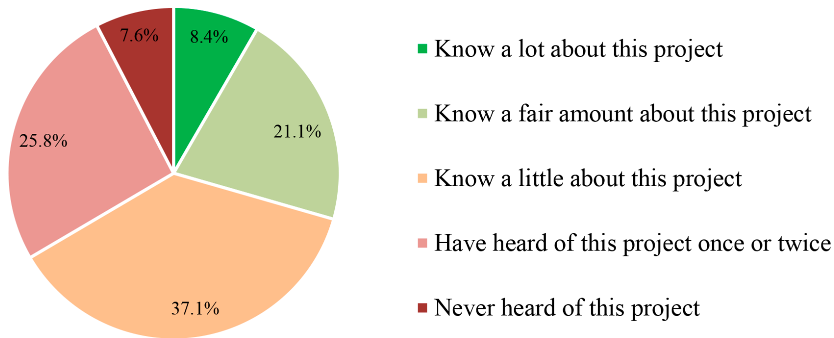

Figure 8.9 Participants' Knowledge of INDOT DWPT Testbed.

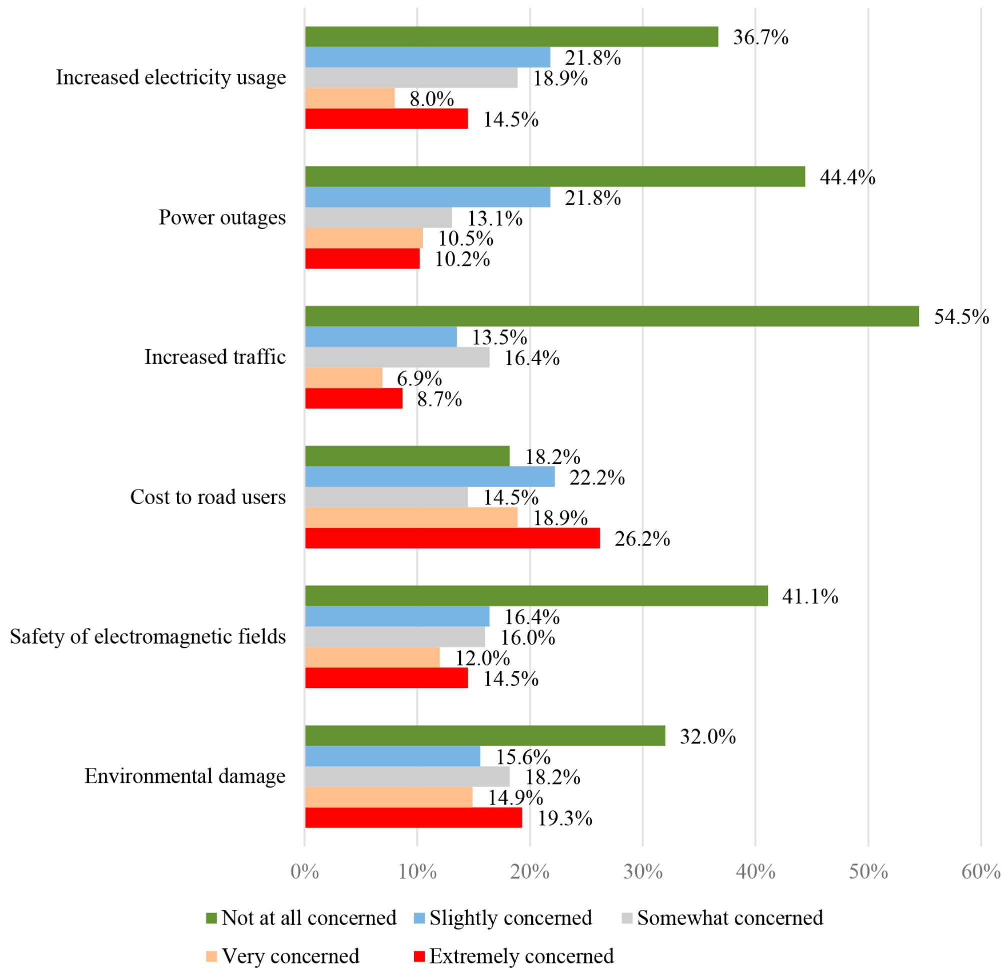

Figure 8.10 Participants' Concerns With DWPT Technology.

through six possible concerns that participants could feel related to electricity usage and power outages, traffic, cost, safety of electromagnetic fields, and environmental damage. Participants reported greater concerns with cost to road users, as more than 80% of the sample reported feeling some level of concern. On the other hand, more than half of the sample stated that they were concerned with the potential increase in traffic related to the technology. Figure 8.10 shows the responses for all six concerns.

8.2.1.3 Concerns with Testbed Construction. Participants were also asked about their construction concerns with the testbed, such as access to sidewalks and transversal lanes, lanes and road closure, and light and noise pollution. Different from the concerns

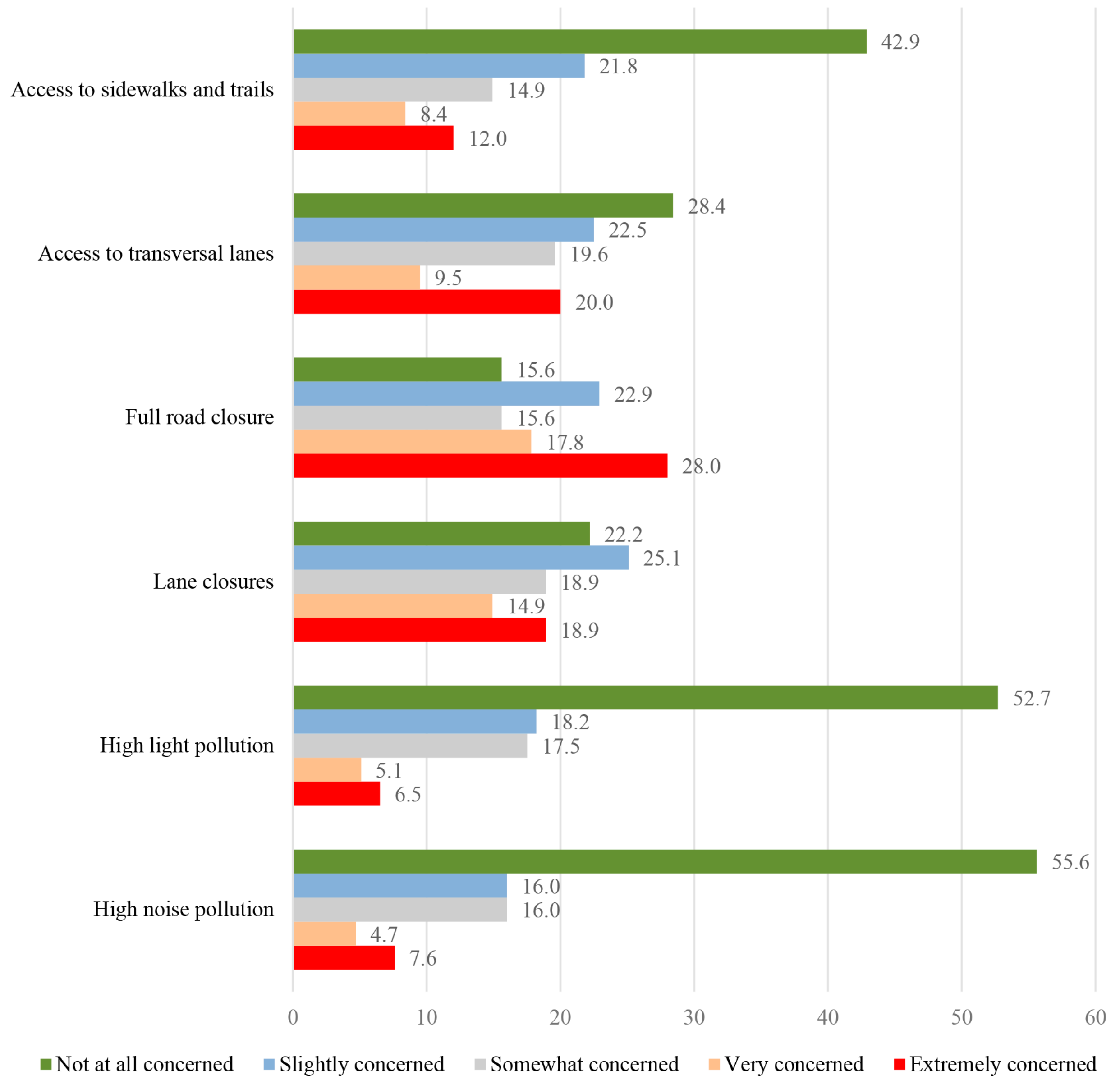

Figure 8.11 Participants' Concerns With the Testbed Construction.

with the technology, for the testbed construction, the participants are particularly concerned with the traffic, as road and lane closure, as well as access to transversal lanes, were the topics that participants felt more concerned about, as shown in Figure 8.11.

8.2.2 Qualitative Results

8.2.2.1 Key Themes of Interest to Respondents. We identified a total of twenty-four topics from our analysis of open-ended comments. The distribution of the finalized thematic coding is shown in Figure 8.12, where larger boxes mean the topic was discussed with higher frequency.

There were three thematic ideas that tied most topics together: economic, health and environment, and EV adoption barriers. There were positive and negative sentiments within each theme, as highlighted in Figure 8.12. On the economic side, participants mentioned financial concerns relative to DWPT construction and roadway usage/maintenance. While respondents agree that investment in public infrastructure is warranted, they emphasized how public spending should support projects that benefit the whole community, such as providing more low-emission public transit options. For now, respondents seem to believe DWPT will mostly benefit EV users, who are a small subset of the larger community. Here are example quotes expressing this view:

- "It seems like a lot of expense and effort for a small group. I understand the drivers will pay for the electricity, but who pays for the construction?"

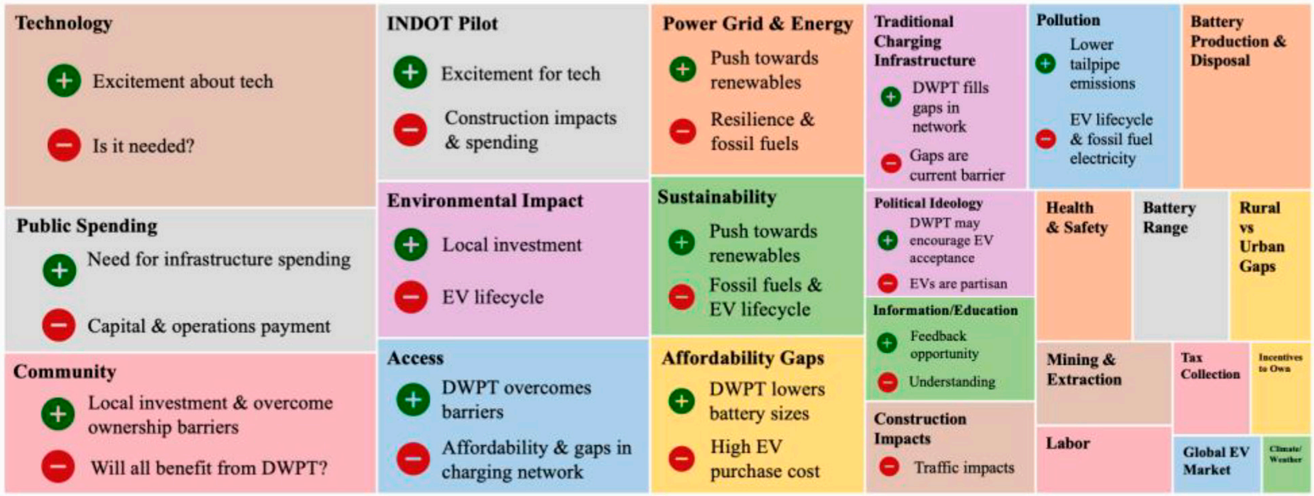

Figure 8.12 Theme Distribution, With Example Positive and Negative Sentiments.

- "I question the efficiency of the wireless charging road and the implementation cost to the public for the benefit of very few."
- "I think at the moment our funds need to be going elsewhere because not many people in the community are able to afford electric cars at this current moment."

Health and environmental themes also emerged. Some respondents believed that EVs and charging infrastructure could help reduce local pollution, while others mentioned concerns related to the potential lifecycle environmental impacts of EVs, such as battery production and disposal, mining, and energy demand. Respondents are also concerned about traffic disruptions resulting from construction of DWPT roadways. Some respondents were positive and felt that DWPT could accelerate a shift to cleaner energy. Here are example quotes highlighting these themes:

- "As far as the full electric goes, it doesn't seem beneficial nor ecologically friendly when you look at the whole process of manufacturing."
- "I like the idea of charging roads. I cannot put into words how much I hate the idea of unnecessary construction to make them happen."
- "My hope is [that] the increased demand for electricity will spur the adoption of more sustainable energy generation facilities, especially nuclear"

Participants also revealed major obstacles to EV adoption, particularly gaps in charging availability and the high upfront cost of EVs. The challenges were noted by people in rural areas or high-density apartment buildings. Some respondents thought DWPT could address these issues by improving access to charging and reducing the need for large batteries. Here are example quotes that explain these themes:

- "I feel that [DWPT] will lower the cost of EVs overall because it will allow for smaller battery sizes."
- "We definitely need more charging stations (or wirelessly charging roads) before people will make the change to EVs. Right now, I'm not sure where I could charge an EV in our community."
- "I live in a small, rural town. While I do think that there are less people in our town that own or lease electric vehicles, I do think that having charging stations and wireless charging in our town or area could encourage people to be more open to owning them in the future. I think that people who seem set in their ways need to actually see the charging stations and wireless charging roads being used so that they can get used to it being an every day thing."

8.2.2.2 Sentiment Distribution of Open-Ended Comments. After running a sentiment analysis across open-ended responses, we found that 57% of respondents expressed negative views (this included views towards issues such as construction, public spending, environmental impact, and DWPT), 13% positive, 14% mixed, 9% neutral, and 7% offered comments that were not related to electric roads or charging (see Figure 8.13). We anticipated high levels of negative feedback at this stage of technology development because the data were collected during pilot construction, which local

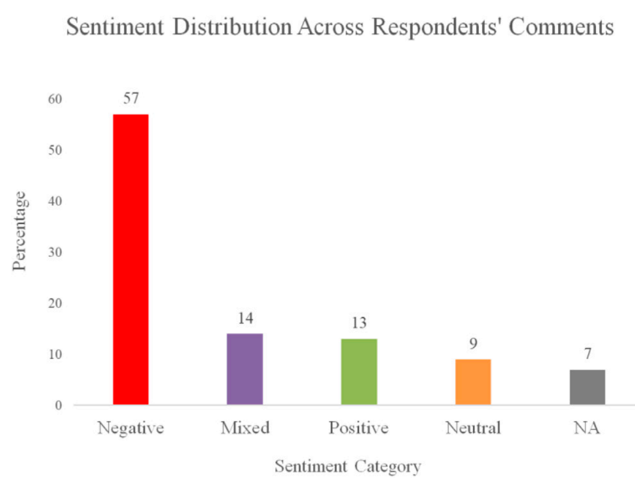

Figure 8.13 Sentiment Distribution of Survey Respondents' Open-Ended Comments.

communities can find distressing, consistent with community acceptance theory (Wüstenhagen et al., 2007). We also observed that the more familiar respondents are with EVs, the more interest and acceptance they display towards DWPT, making education outreach for this new technology particularly important for boosting acceptance among non-EV users or connoisseurs.

Moving forward, clear communication is necessary for the public to understand the benefits DWPT can bring to the local community beyond improving charging for current EV users. Keeping the public engaged with outreach initiatives and informed through education programs about DWPT entering their communities is important for reducing negative perceptions and improving social acceptability of this new technology.

Note that the study has several limitations, including a self-selected, higher-income, and highly educated sample that was not representative of the broader population, limiting generalizability. It also focused on a single local community and captured perceptions at one point in time—during construction—when concerns may have been amplified and benefits underemphasized. Future research should use larger, more representative samples, conduct follow-up surveys after implementation, and specifically examine nearby residents and commercial EV stakeholders to better understand evolving perceptions of DWPT.

9. DWPTT ELECTROMAGNETIC PERFORMANCE TESTING (TASK 7)

In November 2025, Purdue University collaborated with the SAE and TDK Corporation to conduct comprehensive electromagnetic compatibility and electromagnetic field characterization of the DWPT system at Utah State University (USU).

TABLE 9.1
Magnetic Field Results.

Position [cm]	B-field [μT_{rms}] H: 4.5[cm]	B-field [μT_{rms}] H: 7.5[cm]
0	9.14	12.32
10	10.05	10.40
20	10.14	10.43
30	9.91	10.12
40	9.43	9.16
50	9.69	9.48
60	10.36	7.11
70	9.47	5.02
80	9.35	8.14
90	9.44	8.09
100	9.45	8.34
110	9.61	8.49
120	10.05	7.84
130	9.49	8.80
140	8.95	8.48

These assessments are critical for the ongoing development of DWPT standards. Measurements were recorded at varying locations around the tx pads while a Cummins Class-8 battery electric vehicle (BEV) operated in both stationary and high-speed dynamic modes. In a representative safety test, a magnetic radiation tester was positioned 60 in. from the edge of the tx pad. As the vehicle traversed the pad at 25 mph with 190 kW of power being transferred, the sensor was shifted in 4-in. increments to map the field distribution. The results shown in Figure 9.1 are the measured flux density values obtained at each position. As shown in Table 9.1, all measured magnetic field levels remained significantly below the International Commission on Non-Ionizing Radiation Protection (ICNIRP) reference limit of 15 μTrms for human safety.

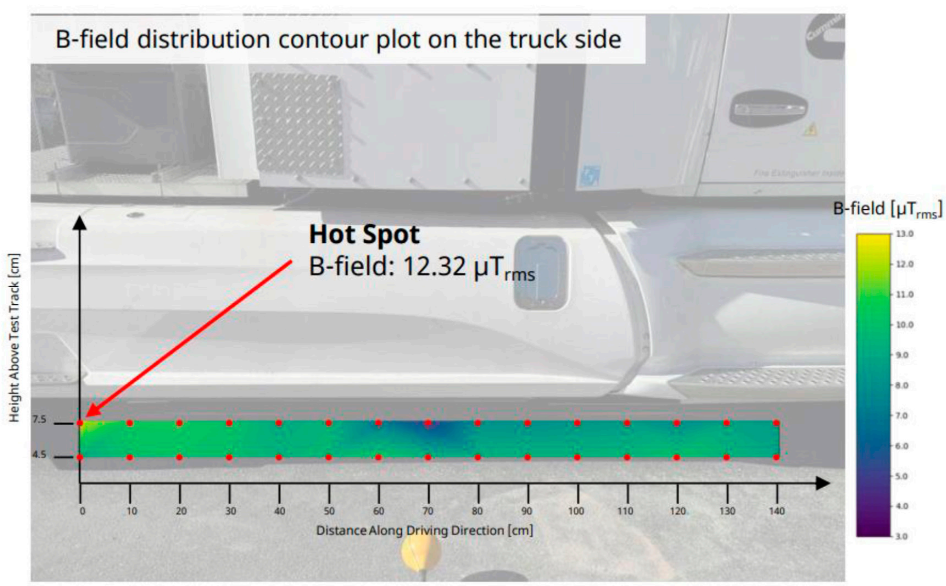

Figure 9.1 B-Field Magnitude Along the Length of the EV.

10. DWPTT INTEROPERABILITY TEST (TASK 8)

DWPT interoperability has two components: vehicle-class interoperability (e.g., passenger cars vs. heavy-duty trucks) and road-class interoperability (e.g., highways vs. lower-speed city roads). A practical way to judge interoperability is the modularity of the DWPT topology—how easily the vehicle-side receiver and the roadway-side hardware can be resized or reconfigured to meet a given vehicle class, battery size, and power requirement. To serve platforms ranging from passenger vehicles to Class 8 (and higher) commercial trucks, a topology should be capable of ~200-kW class transfer while still operating efficiently at 30–50 kW, which is more typical for lighter-duty applications. Road-class interoperability also requires the system to function across a range of vehicle speeds.

Across inductive DWPT approaches, two major design variables drive interoperability: (1) the number of phases and (2) the orientation of magnetic poles. Many systems use poles aligned parallel to the direction of travel, whereas Purdue's design uses transverse poles, which enables straightforward lengthwise scaling of the receiver to increase or decrease power capability. In addition, three-phase architectures reduce rectified power ripple, improve stability under misalignment, and provide the power density needed for heavy-duty vehicles. Three-phase systems also offer a compatibility path to single-phase coils with relatively minor control adjustments. While such cross-compatibility is not as efficient as nominal operation, it can still enable operation between systems with significant design differences.

To evaluate vehicle-class interoperability on the INDOT pilot, the team tested three receiver designs across a wide range of commanded power setpoints. This testing demonstrated operation from ~20 kW (passenger-vehicle relevant) up to ~200 kW (Class-8 relevant). The results also showed that modest changes to the vehicle-side assembly can adjust output characteristics without requiring changes to the roadway-side installation. In trailer-based testing, receiver height was varied to approximate typical passenger-vehicle clearances (6–8 in.) and heavy-truck clearances (8–12 in.).

To evaluate road-class interoperability, dynamic tests were conducted across speeds from ~20 mph to ~65 mph. Although low-speed operation was not the primary design point, the system consistently detected the receiver and delivered power, indicating suitability not only for highway corridors but also for lower-speed roadways.

Finally, reproducibility was assessed by constructing a second testbed at the USU's Electric Vehicle Roadway (EVR) facility. Testing at EVR produced performance comparable to, and in some cases better than, the INDOT site. As shown in Figure 10.1, representative tests at 150 kW and 190 kW have much smoother power profiles, likely due to the decreased voltage dip during pad transitions. This behavior was expected, as the pads for this specific installation were intended to be placed much closer together than the INDOT pilot. Future interoperability work may include reduced-size vehicle receivers, different pavement materials, and single-phase receiver coils. Longer-term, broader interoperability will require standards-driven alignment of key design and test requirements; recent SAE-focused testing is an initial step toward defining which design choices can be standardized.

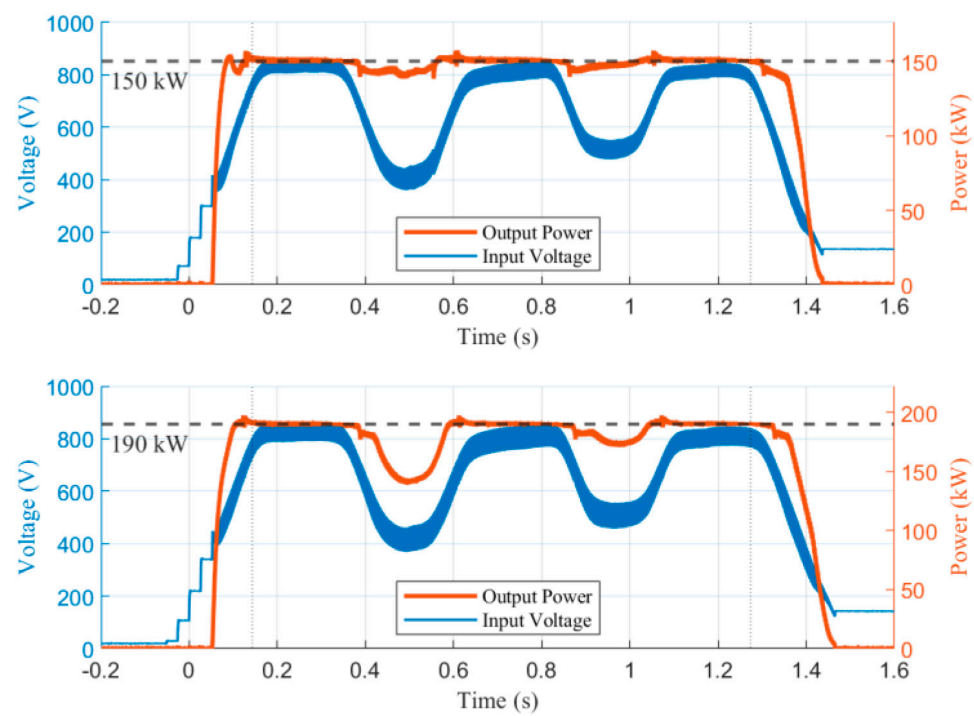

Figure 10.1 Experimental Measurements of Receiver Voltage and Delivered Power.

11. ECONOMIC ASSESSMENT OF DWPT SYSTEMS (TASK 9)

An issue that has been raised in preparing the DWPTT is the respective cost of the system. The high cost is partly because the team made several decisions to minimize risk, including using an inverter for each transmitter coil, rather than using an inverter to serve multiple coils. Purdue has developed a new approach to the inverter/compensation circuit design that we believe will drastically reduce the cost of DWPTT systems going forward by reducing the number of inverters that are required. Specifically, researchers believe a reduced-inverter DWPT system can be developed wherein a single inverter, with some relatively low-cost enhancements to the compensation circuits, can serve multiple (5–10) coils.

Purdue has designed and simulated the performance of the reduced-inverter topology, and it appears to perform well. Purdue has also performed a cost analysis/comparison based upon the reduced-inverter design. For the cost analysis, Purdue has leveraged information from contractors to indicate a reasonable price for a commercialized inverter of $7,500, which is already much less than the prototype-stage inverters (~$20,000) used in the pilot installation. A reduced-inverter DWPTT is shown, along with the existing DWPTT (priced at $7,500/inverter), in Figure 11.1; respective costs are shown in Table 11.1. The Purdue research team is presently completing simulations and hardware setups to evaluate the system behavior.

Additional cost reductions can be achieved through optimization of system layout. One of the inverter/compensation circuit layouts is shown in Figure 11.2. In this configuration the inverters and the compensation circuits corresponding to four different tx pads are placed within one vault. The system consists of a 12-phase inverter unit, and four compensation circuits tune either for tx coils with shorter leads or for the tx with longer lead length. Such arrangement significantly reduces the cost associated with inverter housings and reduced total number of vaults utilized. Incorporating the compensation circuit component separate from the inverter also enhances serviceability of the system. Additionally, this leads to thermal decoupling of the inverters from compensation circuits; considerably reducing the cooling requirement for the inverters and therefore their cost. The cost reduction obtained from such a system layout is expected to be around $3.5- to $4- million per mile compared to the layout strategy employed at the US 52/231 INDOT DWPT pilot.

TABLE 11.1
Per-Mile Cost of a DWPTT System (Assuming a Cost of $7,500/Inverter).

	Initial System			Reduced Inverter System		
Component	**Qty**	**$/ea.**	**$**	**Qty**	**$/ea.**	**$**
Inverter	352	7,500	2,640,000	70	7,500	525,000
Vault	176	8,000	$1,408,000	35	4,000	140,000
Additional Circuitry	0			352	1,000	352,000
Litz wire			400,000			600,000
Total Cost			$ 4,448,000			$ 1,617,000

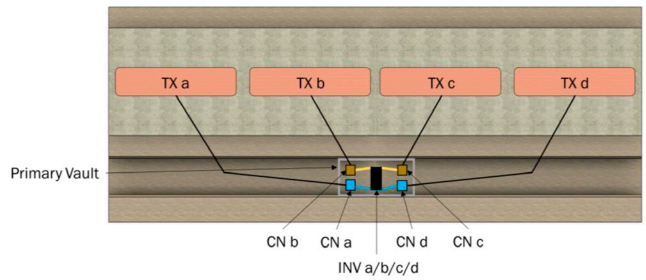

Figure 11.2 Cost Reduction Through System Layout Optimization.

12. CONCLUSIONS

This research demonstrated the feasibility of a high-power DWPT system capable of transferring power to a Class-8 freight vehicle at highway speeds. A novel three-phase transmitter/receiver topology was developed to address the fundamental challenges of freight-scale DWPT: delivering ~180 kW of power, embedding transmitter coils beneath the pavement surface to preserve maintainability, and maintaining sufficient roadway-to-receiver ground clearance for vehicle integrity. The resulting system was successfully instantiated in an 85-coil testbed on US 52/231 in West Lafayette, Indiana, with transmitter coils embedded 2.4 in. below an existing concrete pavement and an 8-in. ground clearance to the receiver mounted on a retrofitted Cummins Class-8 tractor.

Technical validation confirmed that all 85 coils met electromagnetic balance specifications, demonstrating that the precise phase separation required for the three-phase topology

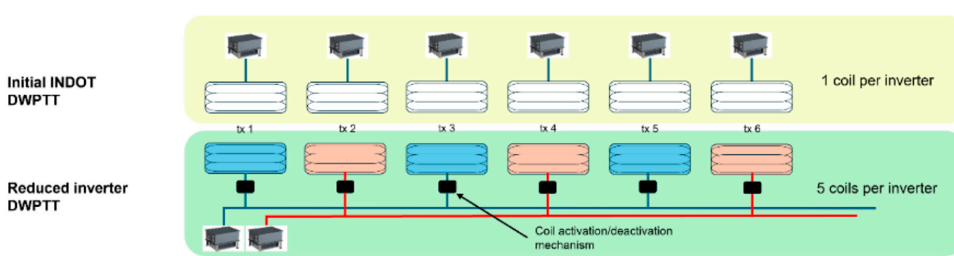

Figure 11.1 Initial INDOT DWPTT and a Reduced-Inverter DWPTT.

can be maintained through multi-stage roadway construction. Most importantly, the system reliably delivered commanded power levels from 50 kW to 190 kW at speeds up to 65 mph, with end-to-end (roadway DC-bus to vehicle DC-bus) efficiencies approaching 85% at peak power. Comparable results were achieved at USU's three-coil testbed, where independent testing confirmed magnetic flux densities well below the 15 μT human exposure threshold. Notably, robust power delivery was achieved without active alignment technologies, underscoring the inherent misalignment tolerance of the three-phase design.

From an implementation perspective, the project provides critical insight into the practical realities of constructing electrified roadway infrastructure. Retrofitting DWPT into existing concrete pavements proved cost prohibitive due to the complexity of milling, conduit placement, and vault installation. Lessons learned point toward more economical strategies for future deployments, including integration into new pavement construction using precast or slip-form approaches, reduction of Litz conductor terminations through neutral-point coil design, consolidation of inverters to serve multiple coils, and use of fast-response battery energy storage systems to stabilize DC-bus transients during commissioning and operation. Collectively, these refinements offer a clear pathway to significant system cost reductions. Equally important, the project demonstrated that public perception is a critical determinant of successful technology deployment. Outreach efforts conducted in partnership with INDOT revealed that community members recognize potential benefits of DWPT, including improved air quality and reduced range anxiety, while also expressing concerns regarding public investment priorities and construction impacts. The findings reinforce the importance of transparent communication, proactive engagement during construction, and framing DWPT as shared infrastructure that addresses tangible barriers to freight electrification.

In summary, this work validates the technical feasibility of high-power, roadway-embedded DWPT for freight applications and establishes a foundation for scalable deployment. While economic optimization and infrastructure integration remain active areas for development, the demonstrated performance, safety compliance, and public engagement outcomes collectively indicate that DWPT represents a promising pathway toward reducing battery size requirements, lowering total cost of ownership, increasing freight asset utilization, and accelerating the decarbonization of heavy-duty transportation.

REFERENCES

Abram, I., Frooninckx, N., Mehar, V., Brovont, A. D., Aliprantis, D., Pekarek, S. D., & Swanson, R. (2025). *Fabrication and characterization of roadway-embedded DWPT transmitter coils* [Conference proceedings]. 2025 IEEE/AIAA Transportation Electrification Conference and Electric Aircraft Technologies Symposium (ITEC+EATS), Anaheim, CA, United States. https://doi.org/10.1109/ITEC63604.2025.11097935

Aliprantis, D., Brovont, A., Gkritza, K., Haddock, J., Pekarek, S., & Swanson, R. (2025). Power on the move: Indiana's high-power dynamic wireless power transfer testbed. *IEEE Electrification Magazine*, *13*(4), 17–29. https://doi.org/10.1109/MELE.2025.3627568

Indiana Department of Transportation. (2024). *Dynamic wireless power transfer*. https://www.in.gov/indot/emerging-mobility/dynamic-wireless-power-transfer/

Mehar, V., Frooninckx, N., Abram, I., Pekarek, S. D., Aliprantis, D., & Brovont, A. D. (2025). *Receiver-side power control of a 200-kW three-phase DWPT system for heavy-duty vehicles* [Conference proceeding]. 2025 IEEE Wireless Power Technology Conference and Expo (WPTCE), Rome, Italy. https://doi.org/10.1109/WPTCE62521.2025.11062153

Moncada, O. A., Imran, Z., Vickers, C., Gkritza, K., Pekarek, S., Aliprantis, D., Brovont, A., Jahangiri, B., & Haddock, J. E. (2024). *Full-scale dynamic wireless power transfer and pilot project implementation* (Joint Transportation Research Program Publication No. FHWA/IN/JTRP-2024/11). Purdue University. https://doi.org/10.5703/1288284317744

Moncada, O. A., Li, J., Orosa, P., & Haddock, J. E. (2025). *Structural modeling and assessment of rigid pavement with embedded dynamic wireless power transfer components* [Conference proceeding]. 2025 IEEE Wireless Power Technology Conference and Expo (WPTCE), Rome, Italy. https://doi.org/10.1109/WPTCE62521.2025.11062229

Park, B., Cho, S., Rahbar-Rastegar, R., Nantung, T. E., & Haddock, J. E. (2024). Use of falling weight deflectometer data to determine the effective structural number of full-depth asphalt pavements for structural condition assessment. *Road Materials and Pavement Design*, *25*(2), 276–290. https://doi.org/10.1080/14680629.2023.2200843

Wüstenhagen, R., Wolsink, M., & Bürer, M. J. (2007). Social acceptance of renewable energy innovation: An introduction to the concept. *Energy Policy*, *35*(5), 2683–2691. https://doi.org/10.1016/j.enpol.2006.12.001

About the Joint Transportation Research Program (JTRP)

On March 11, 1937, the Indiana Legislature passed an act which authorized the Indiana State Highway Commission to cooperate with and assist Purdue University in developing the best methods of improving and maintaining the highways of the state and the respective counties thereof. That collaborative effort was called the Joint Highway Research Project (JHRP). In 1997 the collaborative venture was renamed as the Joint Transportation Research Program (JTRP) to reflect the state and national efforts to integrate the management and operation of various transportation modes.

The first studies of JHRP were concerned with Test Road No. 1—evaluation of the weathering characteristics of stabilized materials. After World War II, the JHRP program grew substantially and was regularly producing technical reports. Over 1,600 technical reports are now available, published as part of the JHRP and subsequently JTRP collaborative venture between Purdue University and what is now the Indiana Department of Transportation.

Free online access to all reports is provided through a unique collaboration between JTRP and Purdue Libraries. These are available at docs.lib.purdue.edu/jtrp/.

Further information about JTRP and its current research program is available at engineering.purdue.edu/JTRP.

About This Report

An open access version of this publication is available online. See the URL in the citation below.

Moncada, O. A., Abram, I., Frooninckx, N., Mehar, V., Cervini, C., O'Brien, B., Moras, B. K., Pekarek, S., Haddock, J. E., Aliprantis, D., Brovont, A., Gkritza, K., & Swanson, R. (2026). *Receiver, vehicle, and roadway systems for a dynamic wireless power transfer roadway testbed* (Joint Transportation Research Program Publication No. FHWA/IN/JTRP-2026/18). West Lafayette, IN: Purdue University. https://doi.org/10.5703/1288284318633